

# Distributed-force-feedback-based reflex with online learning for adaptive quadruped motor control

Tao Sun<sup>a,b</sup>, Zhendong Dai<sup>a</sup>, Poramate Manoonpong<sup>a,b,\*</sup>

<sup>a</sup>*Institute of Bio-inspired Structure and Surface Engineering, College of Mechanical and Electrical Engineering, Nanjing University of Aeronautics and Astronautics, Nanjing, China*

<sup>b</sup>*Embodied AI & Neurorobotics Lab, SDU Biorobotics, the Mærsk Mc-Kinney Møller Institute, the University of Southern Denmark, Odense M, Denmark*

---

## Abstract

Biological motor control mechanisms (e.g., central pattern generators (CPGs), sensory feedback, reflexes, and motor learning) play a crucial role in the adaptive locomotion of animals. However, the interaction and integration of these mechanisms—necessary for generating the efficient, adaptive locomotion responses of legged robots to diverse terrains—has not yet been fully realized. One issue is that of achieving adaptive motor control for fast postural adaptation across various terrains. To address this issue, this study proposes a novel distributed-force-feedback-based reflex with online learning (DFRL). It integrates force-sensory feedback, reflexes, and learning to cooperate with CPGs in producing adaptive motor commands. The DFRL is based on a simple neural network that uses plastic synapses modulated online by a fast dual integral learner. Experimental results on different quadruped robots show that the DFRL can (1) automatically and rapidly adapt the CPG patterns (motor commands) of the robots, enabling them to realize appropriate body postures during locomotion and (2) enable the robots to effectively accommodate themselves to various slope terrains, including steep ones. Consequently, the DFRL-controlled robots can achieve efficient adaptive locomotion, to tackle complex terrains with diverse slopes.

---

\*Corresponding author

Email addresses: [s.tao@nuaa.edu.cn](mailto:s.tao@nuaa.edu.cn) (Tao Sun), [zddai@nuaa.edu.cn](mailto:zddai@nuaa.edu.cn) (Zhendong Dai), [poma@nuaa.edu.cn](mailto:poma@nuaa.edu.cn) (Poramate Manoonpong )

*Keywords:* Reflexes, CPGs, Motor learning, Offset adaptation, Slope terrains, Quadruped robots.

---

## 1. Introduction

Animals show elegant locomotion with impressive adaptation, and this has been the primary source of inspiration for developing advanced robot locomotion control [1]. To date, certain quadruped robots (such as SpotMimi<sup>1</sup>, Laikago<sup>2</sup>, ANYmal [2], MIT cheetah [3], LittleDog [4], and HyQ2Max [5]) have demonstrated excellent locomotion behaviors. However, their controllers are based on classical engineering control techniques (e.g., whole body control [6], inverse dynamic model-based control [4], optimization-based control [7], and nonlinear model predictive control (MPC) [8]), which rely heavily on precise/specific dynamic or kinematic robot models and their environments. Thus, their control performance depends highly on the quality of the model. These techniques also require extensive knowledge and intensive computation for control parameter optimization. Moreover, it is still difficult to relate the robot techniques to their biological counterparts and understand the biological locomotion control mechanisms involved.

Therefore, the development of genuine bio-inspired control without reliance on robot and environment models not only has potential for successfully mimicking dexterous animal-like locomotion with computational efficiency, but it also provides a basis for validating a hypothesis in biological investigation [9].

Central pattern generators (CPGs) for generating rhythmic synchronized patterns and reflexes with sensory feedback to realize adaptation of the patterns play a crucial role in the control of animal locomotion [10, 11, 12, 13, 14]. However, the interaction and integration among these mechanisms for generating efficient adaptive locomotion on complex terrains remain under investigation

---

<sup>1</sup><https://www.bostondynamics.com/spot>

<sup>2</sup><https://www.unitree.cc>

in robot locomotion [10, 15, 16, 9]. Although certain existing CPG-based controls include CPG phase adaptation for generating adaptive gaits [17, 18] and CPG frequency adaptation for generating efficient stepping frequency [19], CPG offset adaptation for obtaining adaptive body posture corresponding to diverse terrains (Fig. 1) has only been partially investigated, as described below.

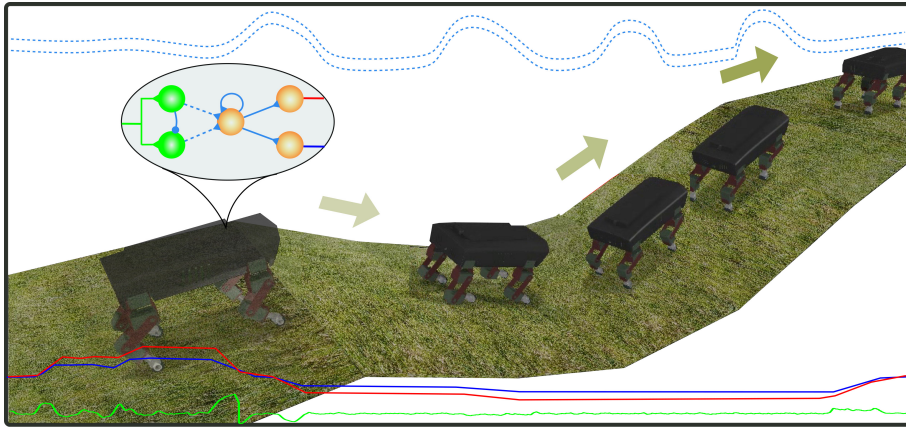


Figure 1: A quadruped robot successfully trots on a complex terrain consisting of multiple slopes. It is driven by the distributed-force-feedback-based reflex with online learning represented by a simplified neural diagram (see circle). The reflex circuit has two plastic synaptic weights (dashed lines projecting from the two input neurons to the hidden neurons in the diagram). The weights are adapted online by a fast learning mechanism. The reflex is stimulated by the ground reaction force (GRF) distribution (green line projecting to the two input neurons in the diagram). Its output neurons generate adaptive knee and hip joint commands (red and blue lines in the diagram, respectively). The adaptive commands enable the robot to trot stably on the terrain. The blue dashed lines above the robot and the green, red, and blue lines below the robot describe the weight adaptations, the change in the GRF, the change in the knee joint offset, and the change of the hip joint offset, respectively, during walking on the terrain.

Fukuoka et al. conducted a groundbreaking study on bio-inspired control for adaptive quadruped walking on irregular terrains. The control is composed of four connected Matsuoka CPGs [20] with sensory feedback to form basic rhythmic patterns and multiple reflexes (i.e., vestibular reflex, flexor reflex, stepping reflex, sideways and corrective stepping reflexes, and crossed flexor reflex). This

35 results in body posture adaptation [16]. However, the reflexes are predefined  
 using several hand-tuned parameters for specific platforms. Such a vestibular  
 reflex [16] (or postural reflex) has also been used, together with various CPG  
 models, for generating adaptive body posture, thus enabling the robot to walk  
 on different slope terrains [21, 22, 23, 24, 25, 26, 27]. Nonetheless, all these  
 40 cases are limited to low slopes (less than  $20^\circ$ , see Table 1). This is because the  
 vestibular reflex utilizes only body posture information (i.e., body orientation)  
 to keep the body parallel to the ground (known as a telescoping strut strategy  
 in biomechanics [28]). To obtain the robot posture balance, its legs must almost  
 fully extend or flex. This leads to leg joint movements near their singular con-  
 45 figuration or joint limits [29], particularly on steep slopes (e.g.,  $30^\circ$ ). Although  
 the traditional vestibular reflex can provide the CPGs with adaptive offsets for  
 balancing body posture, these rely on elaborately predefined control parameters  
 and still have limited ability on high and complex slope terrains (Table 1) (see  
 also the Experiments and Results section).

Table 1: The maximum slope to which robots can adapt based on vestibular reflex modulation.

Works	Year of publication	Max. slope [degree]
Xiuli Zhang et. al. [23]	2008	Around 11.2
Mostafa Ajallooeian et. al. [25]	2013	11.85
Duc Trong Tran et. al. [21]	2014	Around 11
Chengju Liu et. al. [22]	2018	Around 12

50 Instead of the vestibular/postural reflex that requires elaborate design with  
 manual control parameter tuning, machine learning, especially reinforcement  
 learning (RL), has been increasingly applied for automatic control parameter  
 tuning. This is because it not only is model free, but it also has a high poten-  
 tial to generate robot agility, complex motor skills, and adaptability to various  
 55 environments [30, 31, 32, 33, 34]. For instance, Hwangbo et al. proposed an RL-  
 based method for training a neural network policy in simulation and transferred  
 it to the quadruped robot ANYmal, which can perform agile and dynamic motor  
 skills [31]. To avoid long training sessions (e.g., nine days for training a normal

locomotion on a floor) resulting from the structural complexity of the neural  
60 network [31], Thor et al. recently presented a novel control framework that transfers CPG signals into desired joint motor commands for robot locomotion by using a radial basis function network with a simplified structure [33]. The network was trained by black box optimization (BBO), which is a variant of the RL-based policy improvement with path integrals (PI2), to generate the desired  
65 commands. Although the framework has the ability to realize adaptive offsets of CPG signals implicitly, it still requires several training sessions (up to 100 min). Such machine learning techniques, while impressive in their own right, typically need 1) a number of training sessions from several minutes to days and 2) careful objective function training scenario designs. Furthermore, they might fail to  
70 deal with situations that have not been trained before (generalization issue).

To overcome the limitations of the aforementioned control techniques (classical engineering, bio-inspired CPGs with reflexes, and machine learning), a novel distributed-force-feedback-based (DFFB) reflex with online learning (DFRL) for fast offset adaptation of a CPG is presented. The DFRL utilizes the distribution  
75 of the ground reaction forces (GRFs) acting on robot feet as sensory feedback. It can stimulate a response modulation on the CPG offsets in real time for posture adjustment and balance. This strategy is called “lever mechanics” in biomechanics [28].

The DFFB reflex is implemented through a simple recurrent neural network  
80 organized in three layers. The key synaptic weights in the network are plastic and adapted or changed over time by a fast online learning mechanism, called “dual integral learner” (DIL) [19]. The DFFB reflex has fast adaptability owing to the learning mechanism (i.e., DIL). This is because the DIL can appropriately modulate the synaptic weights of the DFFB reflex network online with respect  
85 to sensory feedback. It is important to note that the plastic weights here are not spike-timing-dependent plasticity (STDP) because their changes rely on an error function of the DIL rather than relative spike timings. Therefore, the DFRL has several advantages over the traditional vestibular reflex [22, 23, 24, 25, 16, 26], including online learning for fast automatic control parameter tuning, posture

90 self-stabilization on various slope terrains, and the ability to handle steep and  
complex slope terrains. Because implementation of the DIL does not require  
manual control parameter tuning for a specific robot platform, the DFRL can  
be simply applied to other robot platforms. To evaluate the performance of  
the DFRL, it was integrated with a simple CPG-based control. This results in  
95 adaptive quadruped motor control (AQMC) (Section 2). A comparison with  
the traditional vestibular reflex shows the superior performance of the DFRL  
for adaptive quadruped locomotion (Section 3). The discussion and conclusion  
are presented in Sections 4 and 5, respectively.

The main contributions of this work are as follows:

- 100 1. A novel bio-inspired reflex mechanism with fast online learning (i.e., DFRL),  
which provides CPG-based control with an offset adaptation function, for  
adaptive body posture corresponding to diverse slopes. Compared with  
the quadruped locomotion control based on classical techniques [4, 6, 8],  
the DFRL with CPG-based control does not require any robot kinemat-  
105 ics and environmental model. Thus, it is more practical. In principle,  
the proposed DFRL based on biological mechanisms is characterized by  
the independence of specific robots and CPG-based control. It provides a  
generic offset adaptation method which can be integrated with different  
CPG models (e.g., special orthogonal group ( $\text{SO}(2)$ ) CPG [35] and dy-  
110 namical movement primitives (DMPs) [36]) for controlling different sized  
and weighted quadruped robots.
2. A demonstration involving quadruped robots with the proposed reflex for  
adaptive body posture to navigate ascending and descending steep slopes  
(i.e.,  $\pm 35^\circ$  for a small robot and  $50^\circ$  and  $-45^\circ$  for a larger one), as well  
115 as a complex terrain with multiple slopes using a trot gait (see Fig. 1).  
This in our knowledge is an advanced achievement in quadruped slope  
locomotion based on reflex mechanisms.
3. A comparison of the performance between the traditional vestibular reflex  
(using the telescoping strut strategy) and the proposed DFRL (using the

<sup>120</sup> lever mechanics strategy) for adaptive quadruped locomotion on various slopes.

4. A possible option for integration and interaction of CPGs, sensory feedback, reflexes, and motor learning. This contributes to better understanding of biological locomotion mechanisms and development of the reflex-based quadruped locomotion control with great adaptability.  
<sup>125</sup>

## 2. Adaptive quadruped motor control (AQMC)

In this section, we introduce the AQMC based on several biological mechanisms (i.e., CPGs, sensory feedback, and reflexes) and online (motor) learning. The control is bio-inspired, model-free, and straightforward, and it offers fast  
<sup>130</sup> control-parameter adaptation. It is derived from the integration of CPG-based control with DFRL (see Fig. 2). The CPG-based control is realized by four identical coupled neural oscillators; meanwhile, the DFRL is realized by a DFFB reflex and DIL. More specifically, the DFFB reflex network projects the sensory inputs to control the motor neurons. Simultaneously, the CPG-based control  
<sup>135</sup> (featuring four identical SO(2)-based CPGs) transmits periodic signals to the motor neurons. Finally, the outputs of the motor neurons control the robot's knee and hip joints. Thus, whilst the CPGs make the joints move periodically, the DFRL control the joint offsets, to facilitate stable locomotion over different slopes (see Fig. 1).

### <sup>140</sup> 2.1. Central pattern generators (CPGs)-based control

We employ a concise and straightforward neural CPG-based control. It involves two basic modules: CPGs and motor neurons (MNs) (Fig. 2). The details are shown in Fig. 3. The CPGs, realized by four neural SO(2) oscillators, are fully coupled via parameters  $\phi_{ij}$  that represent the CPG phase relationship.  
<sup>145</sup> Each neural SO(2)-based CPG has two outputs, which are sent to the peripheral MNs (M1 and M2).

As shown in Fig. 3 (b), the neural SO(2)-based CPG is a recurrent neural network. It consists of two fully connected neurons (N1 and N2). The neurons

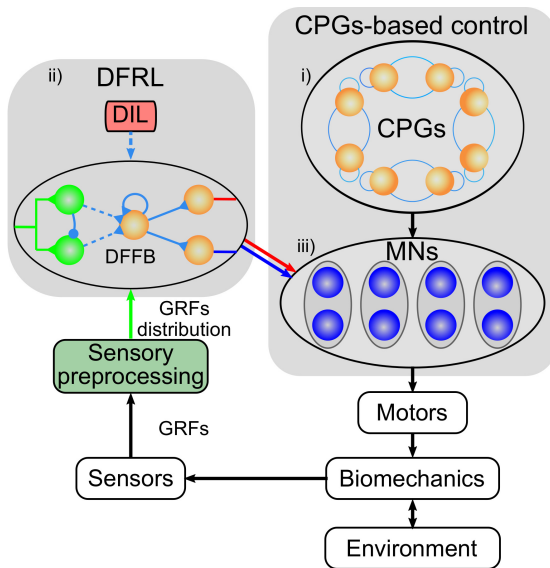


Figure 2: Schematic diagram of the AQMC, featuring (i) a CPG network for producing rhythmic commands; (ii) the DFRL, which includes the DFFB reflex and DIL and uses the GRF information for the CPG offset adaptation; and iii) the MNs for integrating and transferring the adaptive commands from the CPGs and DFFB reflex to drive the robot's leg-joint movements.

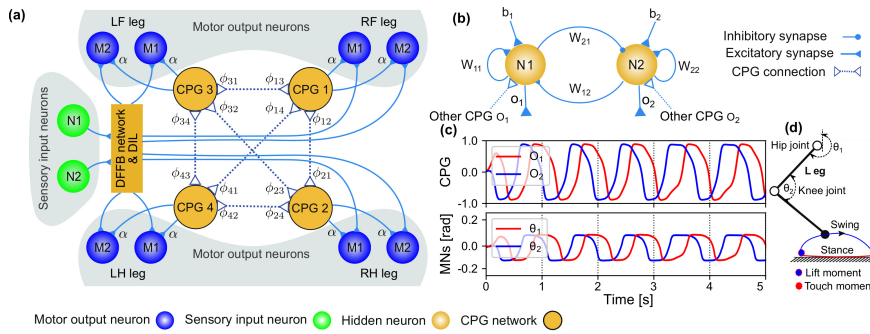


Figure 3: CPG-based control. Four identical CPGs are fully connected via the coupling parameters  $\phi_{ij}$ , which represent CPG phase relationships. Their outputs are sent to four groups of MNs ( $M_1$  and  $M_2$ ) through the synaptic weights  $\alpha$ , to control the four legs' movements. The MNs integrate the DFFB network outputs, triggered by sensory feedback and CPG outputs. (b) The CPG is based on the  $SO(2)$  neural oscillator, which is a recurrent neural network with two neurons ( $N_1$  and  $N_2$ ); these neurons feature internal neural connections (i.e.,  $w_{ij}$ ) and receive inputs from the corresponding neurons of the other CPGs (dashed lines). Each CPG produces two outputs ( $o_1$  and  $o_2$ ) with a fixed phase shift  $\pi/2$ . (c) The outputs of the CPG and MNs of a leg. The MN outputs ( $\theta_1(n)$  and  $\theta_2(n)$ ) send the frequency, waveform, phase, and offset of the CPG outputs ( $o_1$  and  $o_2$ ) to the robot joints. The amplitudes of the MN outputs are scaled by  $\alpha$ -projecting from the CPGs to MNs (e.g., 0.16 for Lilibot and 0.12 for Laikago) to determine a particular step length. (d) Foot trajectory formed under MN outputs. Ideally, the trajectory has four states: lift moment, touch moment, swing phase, and stance phase.

are modeled in time-discrete dynamics using difference equations [35]. Their  
<sub>150</sub> activation function is a hyperbolic tangent ( $\tanh$ ) function, expressed as follows:

$$\mathbf{a}(n+1) = \mathbf{w} \cdot \mathbf{o}(n) + \mathbf{b} + \mathbf{g}(n), \quad (1)$$

$$\mathbf{o}(n) = \tanh(\mathbf{a}(n)). \quad (2)$$

Here,  $\mathbf{a}(n)$ ,  $\mathbf{o}(n)$ , and  $\mathbf{b} \in \mathbb{R}^{2 \times 4}$  represent the activations, outputs, and biases of the CPG neurons, respectively. Note: each column of the matrices represents the state variables of a CPG. The biases are constant, which generates the initial activation of the CPG neurons in accordance with a periodic pattern (i.e., the  
<sub>155</sub> neural dynamics of the CPG are those of a quasi-periodic attractor); their values can be set within the small range of  $-0.085 - 0.085$ . Note: setting them to a larger positive or negative value will drive the neural dynamics to, for example, a fixed point attractor, resulting in constant CPG activities.  $\mathbf{w} \in \mathbb{R}^{2 \times 2}$  denotes the synaptic weights between the two neurons of the neural SO(2)-based CPG.  
<sub>160</sub> Each CPG model has four synaptic weights ( $w_{12}$ ,  $w_{21}$ ,  $w_{11}$ , and  $w_{22}$ ) and two bias terms ( $b_1$  and  $b_2$ , Fig. 3 (b)) The weights and bias terms are empirically set such that the CPG generates two stable periodic signals ( $o_1$  and  $o_2$ , Fig. 3 (b)). The two outputs have a stable phase shift  $\pi/2$  between them, thereby realizing the intralimb coordination of a leg (i.e., the joints of the leg move coordinately)  
<sub>165</sub> [18].

The input data of the CPG neurons is a discrete-time series which is provided to them at each time step ( $n$ ). Here,  $n$  denotes discrete time with an update frequency of 60 Hz. Each neuron features a nonlinear activation function (i.e., a hyperbolic tangent ( $\tanh$ ) transfer function). At each time step, the neuron  
<sub>170</sub> inputs are multiplied by the input weights ( $\mathbf{w}$ ) and summed to obtain the neuron activations ( $\mathbf{a}(n)$ ). Next, the activations are transformed to produce the outputs ( $\mathbf{o}(n)$ ) via the activation function ( $\mathbf{o}(n) = \tanh(\mathbf{a}(n)) \in [-1, 1]$ ). This process is updated at each step.

The four neural SO(2)-based CPGs are fully connected via parameters  $\phi_{ij}$ ,

which represent CPG phase relationships. To generate a trot gait, the inter-CPG connections are also predefined based on a phase-locked function of distributed oscillators [37]; such functions are widely employed for interactions (e.g., phase locking) in oscillator network systems [37, 38, 39, 40, 41]. Here, the inputs delivered to one CPG neuron from other CPG neurons are modeled and described via the term  $\mathbf{g}(n) = (g_{il}(n)) \in \mathbb{R}^{2 \times 4}$  in the CPG model (see Eqs. (1) and (3)).  $g_{il}(n)$  is given by

$$g_{il}(n) = \xi \sum_{k=1}^4 (\sin(o_{il}(n) - o_{ik}(n) - \phi_{lk})) , \quad (3)$$

where  $o_{il}(n)$  and  $o_{ik}(n)$  are the outputs of the  $i$ -th neuron in CPG  $l$  and CPG  $k$ , respectively.  $\xi$  is a communication gain that is empirically set to 0.01.  $\phi_{lk}$  is the desired relative phase of CPG  $k$  with respect to CPG  $l$ . For instance, if we set the right-front leg's CPG (CPG 1) in anti-phase to the right-hind leg's CPG (CPG 2), then  $\phi_{21} = \pi$  and  $\phi_{12} = -\pi$ ; if they are in phase, then  $\phi_{12} = 0$  and  $\phi_{21} = 0$ . For a trot gait, the diagonal legs move in phase but in anti-phase with the other legs. Thus, the relative phases between the CPGs under the trot gait are set as

$$\Phi = \begin{pmatrix} \phi_{11} & \phi_{12} & \phi_{13} & \phi_{14} \\ \phi_{21} & \phi_{22} & \phi_{23} & \phi_{24} \\ \phi_{31} & \phi_{32} & \phi_{33} & \phi_{34} \\ \phi_{41} & \phi_{42} & \phi_{43} & \phi_{44} \end{pmatrix} = \begin{pmatrix} 0.0 & -\pi & -\pi & 0.0 \\ \pi & 0.0 & 0.0 & \pi \\ \pi & 0.0 & 0.0 & \pi \\ 0.0 & -\pi & -\pi & 0.0 \end{pmatrix}. \quad (4)$$

$\phi_{lk}$  determines the interlimb coordination or walking pattern. Optimizing this parameter can allow the robot to realize different gaits, which can enhance its performance under certain conditions. However, in this study, the parameter was predefined to produce a trot gait without further gait optimization.

The MNs are used to convert the CPG outputs into the desired joint movement commands. Their transfer functions are also tanh functions; this allows the MNs to capture the main features of the CPG outputs, such as the frequency, waveform (i.e., duration of the ascending and descending phases within a cycle), phase relationships among the outputs, and offsets. The amplitudes of

the MN outputs can be set via the synaptic weight projection from the CPGs to the MNs ( $\alpha$ , see Fig. 3 (a)). As a result, the CPG outputs are properly mapped to the joint angles, and the robot feet will exhibit alternating stance and swing motion states when the robot is balanced at the lift/touch moment (Fig. 3 (d)). The MNs are defined as

$$\boldsymbol{\theta}(n) = \tanh(\alpha \mathbf{o}(n) + \boldsymbol{\beta}(n)), \quad (5)$$

where  $\mathbf{o}(n)$ ,  $\boldsymbol{\beta}(n)$ , and  $\boldsymbol{\theta}(n) \in \mathbb{R}^{2 \times 4}$ .  $\boldsymbol{\theta}(n)$  is the joint command,  $\mathbf{o}(n)$  is the CPG output,  $\alpha$  represents the synaptic weight projection from the CPGs to the MNs (e.g., 0.16 for Lilibot and 0.12 for Laikago, see Fig. 3 (c)).  $\boldsymbol{\beta}(n)$  denotes the joint command offsets and determines the robot-joint offsets required to set the robot body posture. In this work, we optimize this parameter using the proposed DFRL (see Fig. 5). Optimizing the parameter  $\boldsymbol{\beta}(n)$  provides the robot with a proper body posture for stable locomotion over various slopes.

### 195 2.2. Distributed-force-feedback-based reflex with online learning (DFRL)

The DFRL is realized by the DFFB reflex and DIL (Fig. 2). The DFFB reflex is organized by a simple neural network with synaptic plasticity; this network can be triggered by the GRF distribution, while the network's plastic synapse strengths can be adapted online by the DIL.

#### 200 2.2.1. Distribution of ground reaction forces (GRFs)

The distribution of GRFs acting upon the robot's feet is an effective index of robot motion stability and efficiency [42, 43, 44]. Here, it is formulated as sensory feedback, which stimulates the DFFB reflex to maintain locomotion stability by adjusting CPG/joint offsets. This realizes adaptable CPG offsets. In the robot model illustrated in Fig. 4 (a),  $F_f$  and  $F_h$  represent the GRFs of the front and hind legs, respectively; meanwhile,  $ma$  is the resultant force acting upon the body in the sagittal plane, which points the zero moment point (ZMP) towards the ground when the robot locomotion is stable [45]. Note: each leg's mass is neglected because it is light in comparison with the robot's body

<sup>210</sup> weight. The ZMP position can be described by  $x_1$  and  $x_2$  in the sagittal plane; from this, a stability index  $\gamma(n)$  can be derived as

$$\gamma(n) = x_1/x_2, \quad (6)$$

where  $x_1$  and  $x_2$  denote the distances between the footholds and the ZMP (see Fig. 4 (a)). Furthermore, we obtain the following equilibrium equation for the robot:

$$x_1 \cdot F_h = x_2 \cdot F_f. \quad (7)$$

Here,  $F_f$  and  $F_h$  are the GRFs of the front ( $f$ ) and hind ( $h$ ) legs, respectively. By combining Eqs. (6) and (7),  $\gamma(n)$  can be conveniently calculated online from the GRF signals measured by the foot force sensors, as follows:

$$\gamma(n) = \begin{cases} F_f/F_h & F_h \neq 0 \\ 0 & F_h = 0 \end{cases}. \quad (8)$$

<sup>215</sup> Therefore, the stability index can also be considered as a metric of the distribution of GRFs. This is the basis of the idea that the DFFB reflex can maintain locomotion stability by using the distribution of GRFs as sensory feedback.

### 2.2.2. Distributed-force-feedback-based (DFFB) reflex

<sup>220</sup> Intuitively, two fundamental and essential motion conditions are involved in the stable trotting gaits of quadruped robots. First, the flight feet must be able to touch the ground in time to support the robot body, to ensure regular alternation (touching condition). Second, the support feet must be able to lift to swing in time when making a step (lifting condition). The first condition can be realized by using either a high step frequency or a small step length. In this work, we focus on the second condition, to handle more complex lifting conditions (e.g., lifting when walking on a slope).

<sup>225</sup> This condition is fulfilled by the proposed DFFB reflex mechanism, which can appropriately redistribute the GRFs on the stance feet by adjusting the body posture with respect to the ground; this allows the support feet to lift

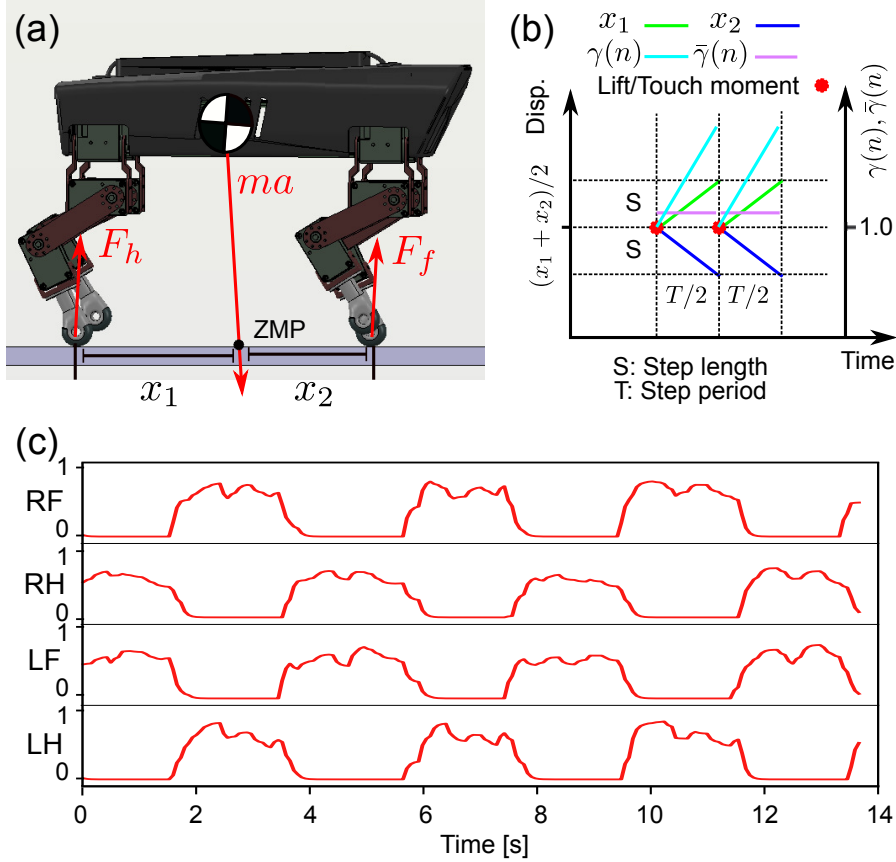


Figure 4: GRF distribution. (a) Force balance of the quadrupedal robot at a moment when its feet all touch the ground. (b) The ideal profile of the parameters  $x_1$ ,  $x_2$ ,  $\gamma(n)$ , and  $\bar{\gamma}(n)$  during a step period whilst the robot stably trots forward; here,  $x_1$  increases while  $x_2$  decreases in every half period. Thus,  $\gamma(n)$  increases significantly from 1.0 at the lift/touch moment.  $\bar{\gamma}(n)$  (see Eq. (9)), obtained by smoothing  $\gamma(n)$ , is a constant value greater than 1.0. (c) The filtered GRFs of four legs for a quadrupedal robot performing stable locomotion via a trot gait. RF, RH, LF, and LH are the right-front, right-hind, left-front, and left-hind legs, respectively.

230 with the desired movement. The desired lifting movement arises from the GRFs  
 between the front and hind legs; ideally, they are approximately equal at the  
 lift moment ( $n = n_0$ ) (see Fig. 4 (b)). This means that  $F_f(n_0) = F_h(n_0)$  or  
 $\gamma(n_0) = 1$  (Eq. (8)), where  $n_0$  indicates the moment at which the stance and  
 swing phases switch. As shown in Fig. 4 (b), the profile of  $\gamma(n)$  is reset to 1.0  
 235 at each lift/touch moment ( $n_0$ ) during ideal trot locomotion. However,  $\gamma(n)$   
 increases significantly in each half-step period following the lift/touch moment  
 ( $n_0$ ). This indicates that the trot gait is not statistically stable. To prevent an  
 unstable situation in which the robot might fall down, the  $\gamma(n)$  value should be  
 reset promptly.

240 However, in reality, it is difficult to precisely determine the touch moment  
 $(n_0)$  and obtain  $F_{f,h}(n_0)$  and  $\gamma(n_0)$  promptly. Therefore, in practice, a smoothed  
 GRF distribution variable ( $\bar{\gamma}(n)$ ) is used for locomotion state estimation and as  
 sensory feedback for the DFFB reflex.  $\bar{\gamma}(n)$  denotes the average value of  $\gamma(n)$   
 during a certain period (Eq. (9)). When a stable trot gait occurs in quadruped  
 245 robots, the  $\gamma(n)$  profile—determined by the specific step length (or joint move-  
 ment range) and period—should be a constant pattern (Fig. 4 (b)). Thus, the  
 corresponding  $\bar{\gamma}(n)$  should be constant. In the following robot experiments, the  
 desired  $\bar{\gamma}(n)$  is  $\sim 1.1$  when the robot stably trots; that is, the joint movement  
 ranges (determined by  $\alpha$ , Eq. (5)) of Lilibot and Laikago are 0.16 and 0.12 rad,  
 250 respectively, while their step periods are  $\sim 1.5$  s.

### 2.2.3. Distributed-force-feedback-based reflex with online learning (DFRL) realization

As shown in Fig. 5, the DFRL consists of three sub-modules: (i) a sensory  
 preprocessing stage, to properly compute the GRF distribution; (ii) a neural  
 255 control network, for implementing the DFFB reflex and transferring sensory  
 stimulation to the motor outputs; and (iii) a DIL, to online-adapt the synaptic  
 strengths of the reflex neural network.

The sensory preprocessing unit calculates the real-time distribution ( $\gamma(n)$ )  
 of the front and hind GRFs ( $F_f$  and  $F_h$ ), which are smoothed by two digital low-

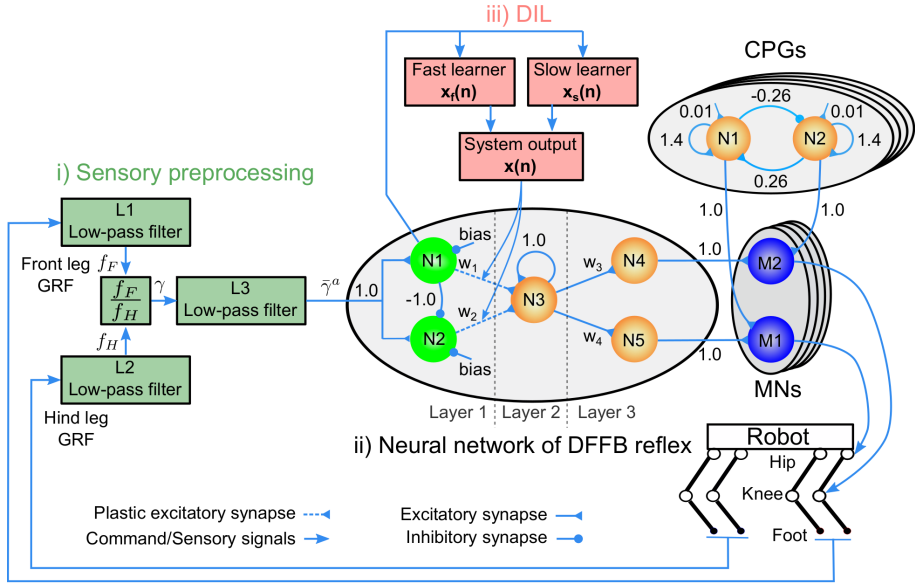


Figure 5: Schematic diagram of the DFRL, featuring three main components: (i) sensory preprocessing, (ii) DFFB reflex network, and (iii) DIL. Sensory preprocessing calculates the actual GRF distribution ( $\gamma(n)$ ) using the front and hind GRFs, which are filtered by two infinite impulse response low-pass filters (L1 and L2 low-pass filters); then, it smooths  $\gamma(n)$  using a moving average filter (L3 low-pass filter) to acquire the actual smoothed GRF distribution  $\bar{\gamma}^a(n)$ , which triggers the reflex network. The DFFB reflex network is organized into three layers (Layers 1, 2, and 3) with five neurons (N1, N2, N3, N4, and N5). It can automatically adapt the knee and hip-joint offsets at MNs. Two plastic synapses ( $w_{1,2}(n)$ ) of the network are online-modulated by the DIL. The biases of the Layer 1 neurons (N1 and N2) represent the desired GRF distribution ( $\bar{\gamma}^d$ ). In the following experiments, they are set to 1.1, depending on the particular step length and period. The synapse ( $w_3$  and  $w_4$ ) projections from the Layer 2 neuron (N3) to the Layer 3 neurons (N4 and N5) were set to 2.0 and 1.0, respectively. Note:  $w_3$  is here set to twice that of  $w_4$  because the foot displacement controlled by the hip joint will be approximately twice of that controlled by the knee joint if the two joints receive the same command values. Therefore, we compensate for this by setting the  $w_3$  value controlling the knee joint to twice the  $w_4$  value controlling the hip joint.

<sup>260</sup> pass single-pole infinite impulse response filters. The GRF distribution ( $\gamma(n)$ ) is then further processed by a two-layer moving average filter to obtain a smoothed RF distribution ( $\bar{\gamma}(n)$ ), as

$$\begin{aligned}\gamma(n)_{temp} &= \frac{1}{N} \sum_{k=n-N}^n \gamma(k), \\ \bar{\gamma}(n) &= \frac{1}{0.5N} \sum_{k=n-0.5N}^n \gamma(k)_{temp},\end{aligned}\tag{9}$$

where  $n$  and  $N \in \mathbb{R}$ .  $n$  indicates the current sample number.  $N$  represents the sample size of the filter; it was empirically set to 50 in the robot experiments.

<sup>265</sup> The DFFB reflex neural network employs the smoothed GRF distribution ( $\bar{\gamma}(n)$ ) as its sensory input, using it to trigger neural network activation. The network consists of three layers: input (Layer 1), hidden (Layer 2), and output (Layer 3). As shown in Fig. 5, the N1 neuron in Layer 1 calculates the difference between the actual and desired GRF distributions ( $\bar{\gamma}^a(n)$  and <sup>270</sup>  $\bar{\gamma}^d(n)$ , respectively). For our setup, the desired value is 1.1, as defined by the bias term (see Fig. 4 (b)). Accordingly, the difference equation is given by  $\Delta\bar{\gamma}(n) = \bar{\gamma}^a(n) - 1.1$ . The N2 neuron calculates the second-order difference. Its formula is  $\Delta\bar{\gamma}'(n) = \Delta\bar{\gamma}(n) - \Delta\bar{\gamma}(n-1)$ . Thus, the synaptic weight projection from N1 to N2 was set to -1. The use of the second-order difference can partially <sup>275</sup> compensate for the delay effect on  $\bar{\gamma}(n)$  produced by the low-pass filters (see L1, L2, and L3 in Fig. 5). This is because the second-order difference—which reflects the change tendencies of the difference—can adjust the DFFB outputs in advance. In Layer 2, the N3 neuron adds two differences via the two plastic synapses ( $w_{1,2}(n)$ ) and accumulates them via a recurrent connection (i.e., 1.0). <sup>280</sup> In Layer 3, the N4 and N5 neurons properly re-scale the offsets to the knee and hip joints of the leg. Thus, the outputs of N4 and N5 ( $o_4^{dfb}(n)$  and  $o_5^{dfb}(n)$ , respectively) are combined with the CPG outputs at the M2 and M1 neurons.  $o_4^{dfb}(n)$  and  $o_5^{dfb}(n)$  are set to the joint command offsets ( $\beta(n)$ ; see Eq. (5)).

This can be described as follows:

$$\begin{aligned}\beta_1(n) &= o_5^{dffb}(n), \\ \beta_2(n) &= o_4^{dffb}(n).\end{aligned}\tag{10}$$

<sup>285</sup> Therefore, the DFFB reflex can automatically adjust the MN output offsets, to maintain proper body posture in accordance with the GRF distribution. As shown in Fig. 6 (a), the offsets ( $\beta_1(n)$  and  $\beta_2(n)$ ) of the corresponding MN outputs ( $\theta_1(n)$  and  $\theta_2(n)$ ) are adjusted online. This leads to the GRF distribution ( $\bar{\gamma}(n)$ ) converging to a desired value (i.e., 1.1, Fig. 5).

<sup>290</sup> In addition, the synaptic weights ( $w_{1,2}(n)$ ) in the DFFB network—which contribute to the adaptation of the joint offsets—are plastic and adjusted online by the DIL. The sensory stimulation changes obtained by N1 serve as the input to the DIL. More specifically, the DIL features two parallel learners with different learning scales [19]. The fast (slow) learner has a higher (lower) learning rate <sup>295</sup> but a lower (higher) retention one. The DIL can be described as

$$\begin{aligned}e(n) &= \Delta\bar{\gamma}(n), \\ x_f(n) &= A_f \cdot x(n-1) + B_f \cdot e(n) + C_f \cdot \int e(n), \\ x_s(n) &= A_s \cdot x(n-1) + B_s \cdot e(n) + C_s \cdot \int e(n), \\ x(n) &= x_f(n) + x_s(n),\end{aligned}\tag{11}$$

<sup>300</sup> where  $x_f(n)$  and  $x_s(n)$  denote the states of the fast and slow learners, respectively;  $A_{f,s}$  are the retention rates;  $B_{f,s}$  and  $C_{f,s}$  are the learning rates; and  $e(n)$  is the difference between the absolute values of the current and previous N1 outputs of the DFFB reflex network. The DIL does not require its parameters to be precisely adjusted to fit specific situations. Its further advantages can be seen in [19]. The sum of the fast and slow learners' states ( $x(n)$ ) is set as the modulation of the synaptic weights  $w_{1,2}(n)$ , as

$$\Delta w_i(n) = x(n), i = 1, 2,\tag{12}$$

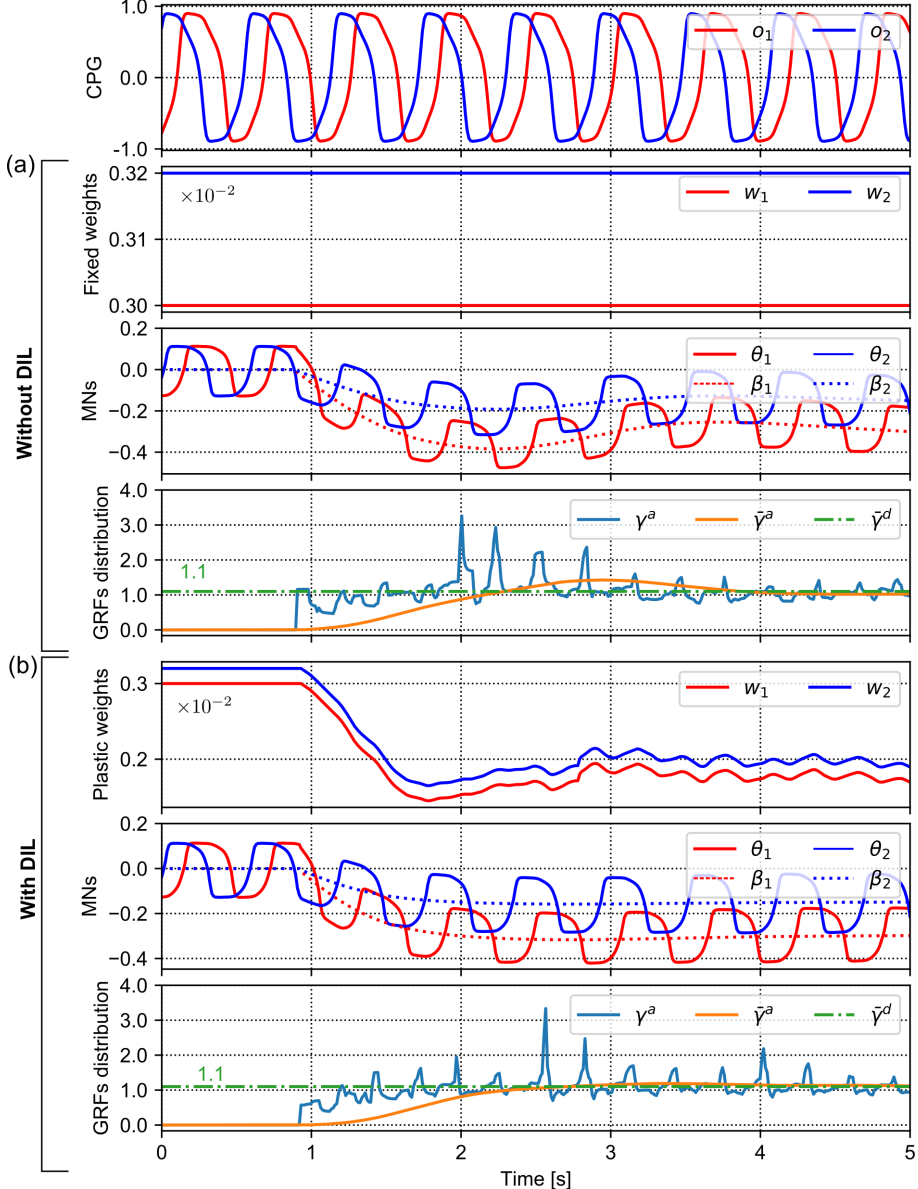


Figure 6: Outputs of the modules ( $o_{1,2}$  from a CPG,  $w_{1,2}(n)$  adjusted by the DIL,  $\beta_{1,2}(n)$  from the DFFB reflex,  $\theta_{1,2}(n)$  from two MN neurons of a leg, and  $\bar{\gamma}(n)$  from the sensory preprocessing unit) in the AQMC. (a) The DFFB reflex without the DIL. (b) The DFFB reflex with the DIL. Using only the DFFB reflex, the offsets of the MN outputs are shifted, and the actual  $\bar{\gamma}^a(n)$  gradually converges to the desired value (i.e.,  $\bar{\gamma}^d \approx 1.1$ ) after  $\sim 4$  s.  $\bar{\gamma}^a(n)$  is also overshot. In contrast, under the DFFB reflex with the DIL, the plastic weights ( $w_{1,2}(n)$ ) are adjusted online to appropriately set the reflex gains. This results in the fast convergence of  $\bar{\gamma}^a(n)$  (within 2 s) and no overshoot. Note:  $\gamma^a(n)$  represents the actual raw GRF distribution.

where the initial values of the weights ( $w_{1,2}(0)$ , see Fig. 5) are empirically set to 0.003 and 0.0032, respectively. This equation shows that the synaptic weights (305  $w_{1,2}(n)$ ) are adjusted online by the DIL’s output ( $x(n)$ ). The DFFB reflex network exhibits synaptic plasticity<sup>3</sup> [46].

This synaptic plasticity provides the reflex network with fast online adaptation, because the DIL can adjust the reflex gains online (i.e., determined by 310  $w_{1,2}(n)$ ) depending on the sensory stimulation changes (see Fig. 6 (b)). For instance, when the input change is large (small), the gains increase (decrease) for realizing adaptive synaptic weights ( $w_{1,2}(n)$ ). This results in joint offset adaptation.

### 3. Experiments and Results

In this study, we performed three main experiments on a small-sized quadrupedal robot (Lilbot [26]) in simulation (Fig. 7), to evaluate the performance of the DFRL for the AQMC. The experiments consisted of (I) trotting on a level ground, (II) trotting on various slopes, and (III) trotting on a complex terrain with multiple slopes (see Fig. 8). The traditional vestibular reflex was also evaluated by implementing it instead of the DFRL for comparison; this reflex utilizes a level-body posture strategy through which the robot body is maintained parallel to the horizontal surface (known as telescoping strut) [16, 47]. This differs from the lever mechanics strategy utilized by the DFFB reflex in 320 the DFRL. The two strategies are shown in Figs. S.7 (b) and (c) in the Supplementary material. The vestibular reflex scheme is outlined in Fig. S.8 of the Supplementary material. In addition to the comparative experiments on Lilbot, the AQMC with the DFRL was also implemented in a larger quadrupedal robot (Laikago, Fig. 7), to demonstrate the DFRL’s generalizability to different platforms.

---

<sup>3</sup>Synaptic plasticity (neuroscientific term): The ability of synapses to strengthen or weaken over time in response to increases or decreases in activity. We import this term to describe the similar abilities of the artificial neural network (DFFB network).

### 3.1. Experimental setup

330 Fig. 7 shows the experimental platforms: Lilibot and Laikago. These two quadruped robots have different sizes, and their specifications can be seen in Table S.2 in the Supplementary material. The robot experiments were performed on three types of terrains, as shown in Figs. 8 (a), (b), and (c). The robots and terrains were simulated using CoppeliaSim<sup>4</sup> with Vortex<sup>5</sup>. These served  
335 as a robot operating system (ROS) node and communicated with the AQMC through certain ROS topics. The simulation platform featuring Lilibot and Laikago can be seen in <https://gitlab.com/neutron-nuaa/lilibot>. The instruction of how to set the parameters of the AQMC can be seen in Section 7 in the Supplementary material.

340 To quantitatively evaluate locomotive performance, three global performance metrics (for a complete locomotion process) were employed to measure the stability, coordination, and displacement of the robot locomotion obtained using the AQMC with the DFRL (DFRL-based AQMC) or vestibular reflex (vestibular-reflex-based AQMC). The metric definitions can be found in Section 6 in the  
345 Supplementary material.

### 3.2. Experiment I: trotting on level ground

350 The CPG/joint offsets significantly influence the robot's posture in terms of trotting stability, coordination, and displacement. The traditional CPG-based control for legged locomotion typically requires the offsets to be predefined robustly. Here, we performed an experiment to verify whether the proposed DFRL allows CPG-based control (Fig. 3) to produce feasible commands with self-adaptive offsets ( $\beta_{1,2}(n)$ ) for maintaining stable locomotion. In addition, the vestibular reflex was tested for comparison.

355 More specifically, the AQMC (with the DFRL or vestibular reflex) was used to control Lilibot's level-ground trot with seven different initial offsets (see Fig.

---

<sup>4</sup><https://www.coppeliarobotics.com/>

<sup>5</sup>A highly realistic and precise physical engine: <https://www.cm-labs.com/vortex-studio/>

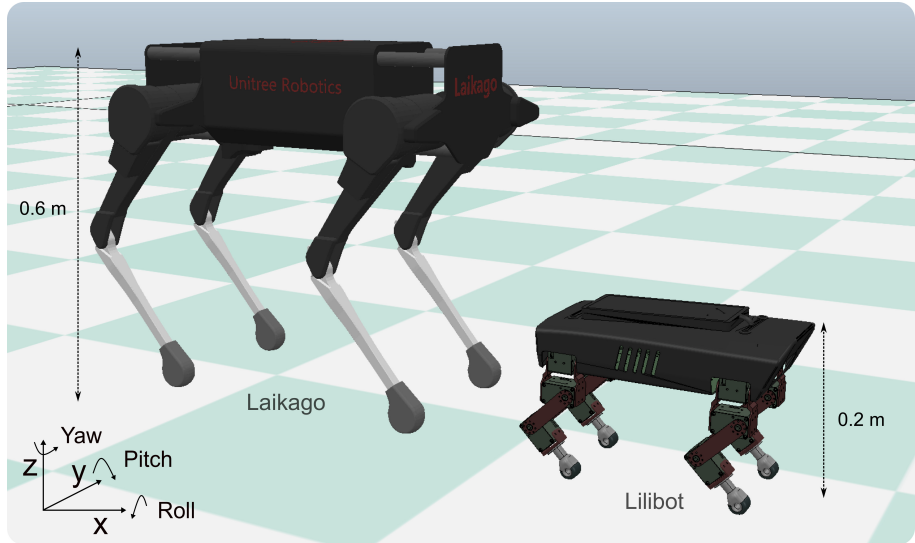


Figure 7: Experimental platforms: Laikago and Lilibot.

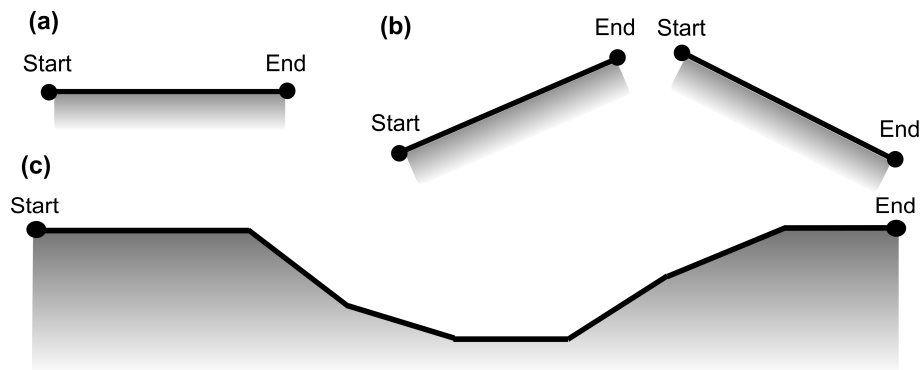


Figure 8: Terrain types used in the three main experiments: (a) level terrain for Experiment I, (b) uphill and downhill terrains for Experiment II, and (c) complex terrain with multiple slopes for Experiment III.

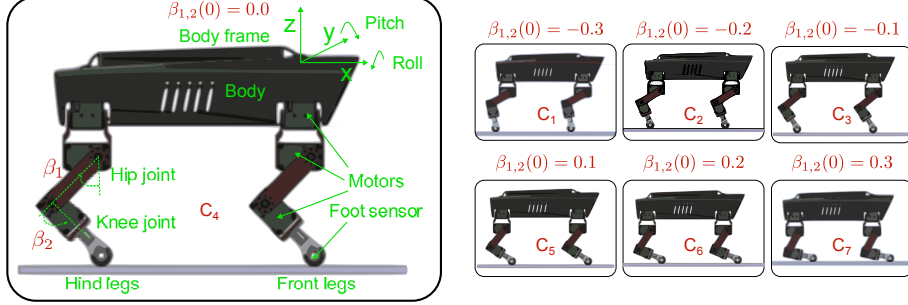


Figure 9: Lilibot configuration and its posture initializations with corresponding joint offsets ( $\beta_{1,2}(n)$ ) in seven conditions ( $C_1, C_2, C_3, C_4, C_5, C_6$ , and  $C_7$ ). The initial values of  $\beta_{1,2}(0)$  were set in the range  $-0.3 - 0.3$ , which covers all possible joint-movement ranges. If the initial offsets ( $\beta_{1,2}(0)$ ) lie outside this range, the robot will fall down. For example, if the value exceeds 0.3, the robot will lean too far forward; if it is smaller than -0.3, the robot will lean too far backward. In both extreme cases, the robot's center of mass will be outside the supporting area of the robot legs, causing it to fall.

9). The corresponding initial offsets of Lilibot's hip and knee joints in the seven conditions  $C_1, C_2, C_3, C_4, C_5, C_6$ , and  $C_7$  were set to -0.3, -0.2, -0.1, 0.0, 0.1, 0.2, and 0.3, respectively. Tests were repeated five times for each condition. At the beginning of every trial, the robot was suspended in the air, to initialize it with identical control parameters. After placing the robot on the ground, the DFRL or vestibular reflex was activated. A video clip of the experiment can be viewed at <http://www.manoonpong.com/DFFB/video1.mp4>.

In this setup, the joints' initial offsets in the  $C_7$  condition show the largest deviation from the normal condition (i.e.,  $C_4$ ). Thus, we include the real-time data for a  $C_7$  (extreme condition) trial as an example. The experimental results are shown in Figs. 10. In the experiments implementing the DFRL, Lilibot rapidly developed a regular trot gait and stably moved forward after interacting with the ground (i.e., within 5 s, Fig. 10 (a)). In addition, the robot body attitude oscillation decreased significantly. On the other hand, a stable gait was not formed in the experiment involving the vestibular reflex, and the robot's hind legs always stalled on the ground (see Fig. 10 (b)). This resulted in a higher body attitude oscillation and smaller forward displacement.

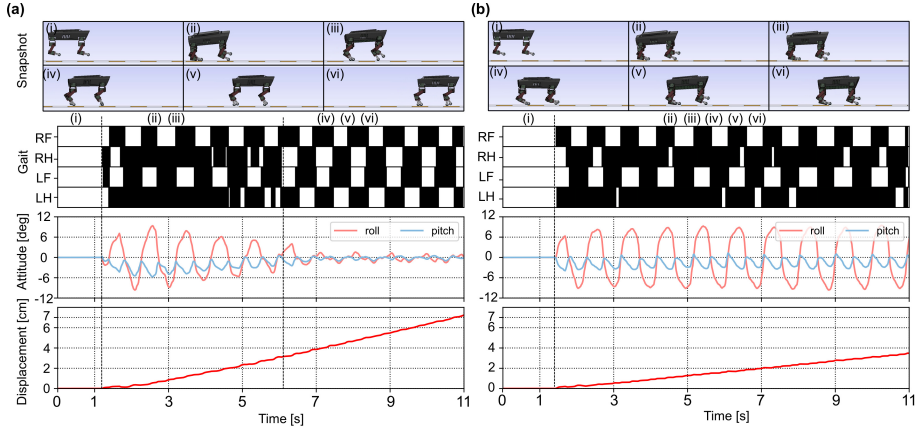


Figure 10: Real-time data for a trial in the  $C_7$  condition, using the (a) DFRL and (b) vestibular reflex. A stable trot gait (with very few body oscillations) emerged after  $\sim 5$  s only when using the DFRL. The black region in the gait diagram indicates the stance phase, whilst the white region indicates the swing phase of each leg (RF, right-front; RH, right-hind; LF, left-front; LH, left-hind).

The convergence progress of tests in all DFRL-based conditions can be seen in Fig. 11. The plastic weights ( $w_{1,2}(n)$ ) of the DFRL are adaptable, which affects the changes in the joint offsets ( $\beta_{1,2}(n)$ ). The joint offsets were online-adjusted by the DFFB reflex of the DFRL (see Eq. (10)); as a result, those of a specific leg (i.e., right-front leg) quickly converged to particular values in all conditions and from different initializations. When the joint offsets were stable, the plastic weights converged to certain values, leading to DFFB reflex gains. In addition, the smoothed GRF distribution parameter ( $\bar{\gamma}(n)$ ) also converged to a constant value of  $\sim 1.1$ . After the offsets became stable, the robot's posture was likewise stabilized (i.e., the roll and pitch angles decrease). However, the results of experiments using the vestibular reflex (see Fig. 12) did not indicate any convergence, and the joint offsets exhibited almost no adjustment. The GRFs distribution values ( $\bar{\gamma}(n)$ ) were spread between 0.0 and 2.0. The robot's posture shows large oscillations under all conditions.

The locomotion performances (*stability, coordination, and displacement*) are shown in Figs. 13 (a), (b), and (c). They demonstrate that the DFRL-based

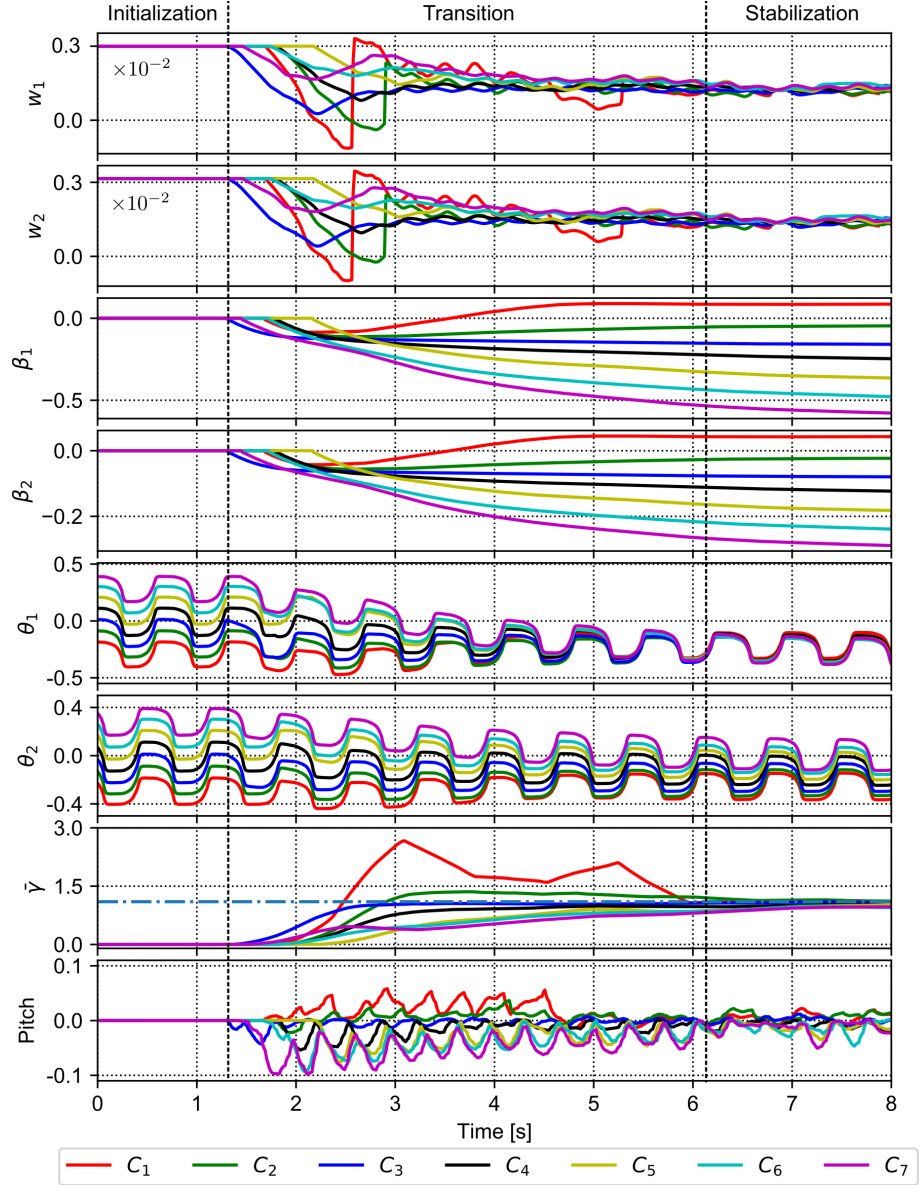


Figure 11: Real-time data for all conditions in Experiment I, using the DFRL. Progress is divided into three stages: initialization, transition, and stabilization.  $w_1(n)$  and  $w_2(n)$  denote the plastic weights of the DFFB reflex network, respectively; these are adjusted online by the DIL (see Eqs. (11) and (12)).  $\beta_1(n)$  and  $\beta_2(n)$  are the hip and knee joint command offsets for a leg (i.e., the right-front leg). They are automatically adjusted by the DFFB reflex (see Eq. (10)). The hip and knee joint commands for the leg are  $\theta_1(n)$  and  $\theta_2(n)$ , respectively. Their offsets converged to constant values within  $\sim 5$  s.  $\bar{\gamma}(n)$  converged to  $\sim 1.1$ . The pitch angle of the robot body—with respect to body stability—became notably smaller following the offset convergence.

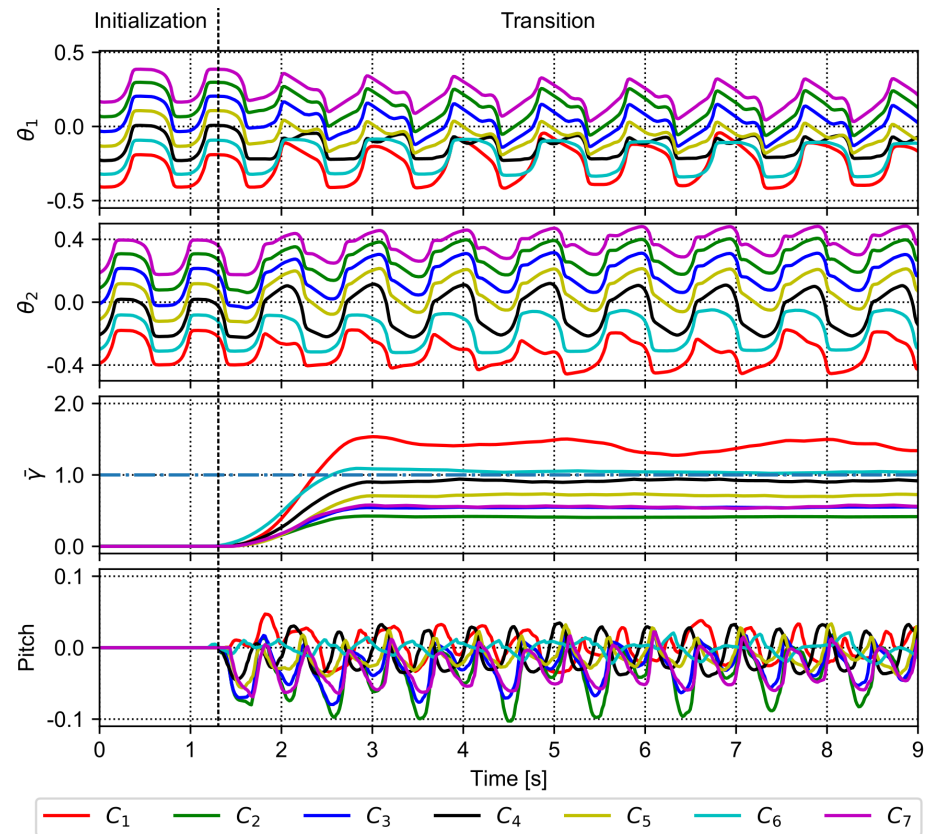


Figure 12: Real-time data for all conditions in Experiment I, using the vestibular reflex. This is for comparison with the DFRL (Fig. 11). In this experiment, no convergence was achieved under any condition.

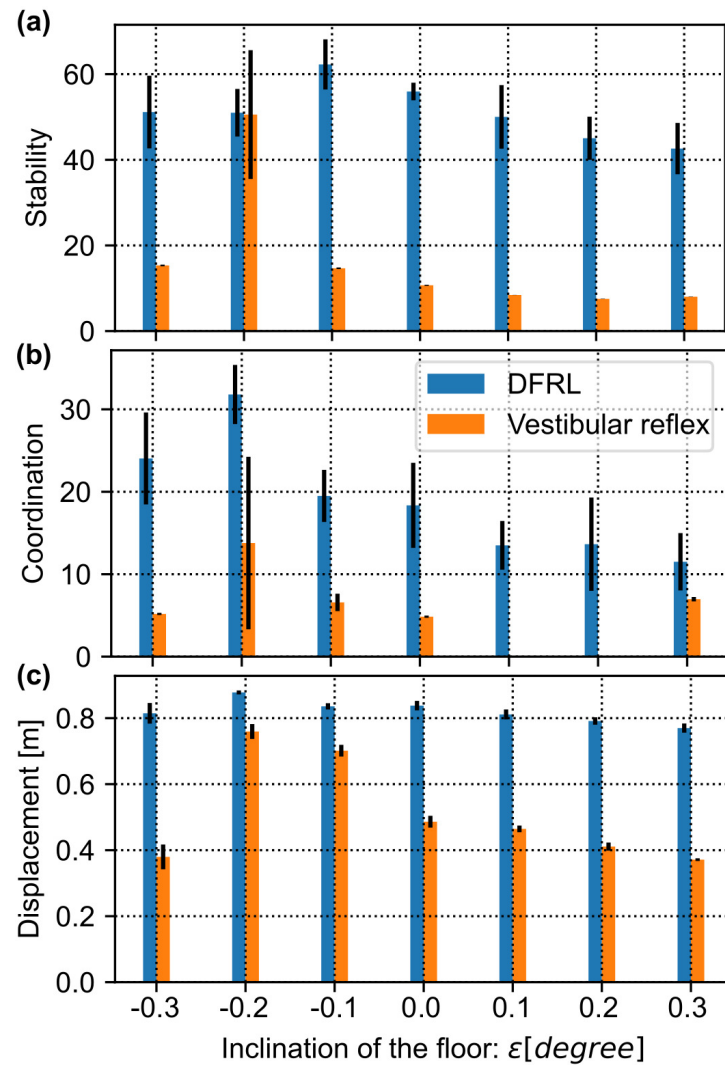


Figure 13: (a) Stability, (b) coordination, and (c) displacement of the robot walking in Experiment I. This demonstrates the comparative results of the DFRL and vestibular reflex.

AQMC enabled Lilibot to realize greater stability and coordination and longer displacement than the vestibular-reflex-based AQMC in almost every test for all conditions. More specifically, the vestibular-reflex-controlled Lilibot only shows sufficient stability under the  $C_2$  condition (-0.2) (see Fig. 13 (a)). The plot in Fig. 13 (b) shows the coordination performance. The DFRL outperformed the vestibular reflex in all conditions. The plot in Fig. 13 (c) shows the displacement. The DFRL-controlled Lilibot traversed an almost-identical displacement under all conditions. However, the most suitable joint offsets for the vestibular reflex only occurred under the  $C_2$  condition. Because the joint offsets of the  $C_2$  condition represent the optimal setup for the vestibular reflex, we used these as the initial offsets for the following slope experiments. To summarize, the results of Experiment I demonstrate that the DFRL allows the robot to rapidly learn and adapt its joint offsets to any initial conditions, facilitating stable trotting over the level ground.

### 3.3. Experiment II: trotting on various slopes

In this experiment, we comparatively assess the effectiveness of the DFRL and vestibular reflex in stabilizing a quadruped robot (i.e., Lilibot) trotting on slopes. A series of slope terrains ( $-35^\circ$ ,  $-30^\circ$ ,  $-20^\circ$ ,  $-10^\circ$ ,  $0^\circ$ ,  $10^\circ$ ,  $20^\circ$ ,  $30^\circ$ , and  $35^\circ$ ) were used for testing. Note: the negative and positive angles denote declined and inclined slopes, respectively. Each test using the DFRL or vestibular reflex on a specific terrain was repeated five times. At the beginning of each trial, the robot was initialized in the same state by suspending it in the air; then, it was placed on the ground to trot forward. Next, it approached a slope with its front legs. The change of the terrain (from the level ground to the slope) presented a challenge for the robot because it needed to adapt its posture to the transition and new terrain, by using its reflex mechanism.

The real-time data for the experiments involving the most challenging slopes ( $35^\circ$  and  $-35^\circ$ ) are depicted first, followed by the experimental statistics for all slopes. A video clip of the experiment can be viewed at <http://www.manoonpong.com/DFFB/video2.mp4>.

### 3.3.1. Feasible maximum slope

When using the DFRL, Lilibot can trot on inclined and declined slope terrains of  $\pm 35^\circ$ . For comparison, real-time data for the vestibular-reflex-controlled robot are also depicted. The adjustment effects of the DFRL and vestibular reflex are shown in Figs. 14 and 15.

The joint commands for a specific leg (i.e., the right-front (RF)),  $\bar{\gamma}(n)$ , body posture angles (i.e., pitch and roll), displacement, and gait diagrams are plotted. Locomotion can be divided into three stages: locomotion on the level ground (S1 stage), transition from the level ground to the slope (S2 stage), and locomotion on the slope (S3 stage).

The experimental results for the  $35^\circ$  slope are shown in Fig. 14. For the S1 and S3 stages under the DFRL (Fig. 14 (a)), the joint commands and  $\bar{\gamma}(n)$  quickly converged after the robot was placed on the ground or crossed the terrain transition.  $\bar{\gamma}(n)$  eventually converged to  $\sim 1.1$ . In addition, the robot pitch angle approximated the slope inclination ( $35^\circ$ ) in the S3 stage. This means that the robot successfully trotted on the  $35^\circ$  slope. The robot roll angle shows very little oscillation during the convergence period (in the S1 and S3 stages). The gradient (velocity) of the displacement curve decreased during uphill locomotion in the S3 stage. This is because the amplitudes of the joint movement commands became smaller and thereby generated a shorter step length. The final gait diagram plot also shows greater regularity during the stabilized stages (S1 and S3), indicating that the robot achieved a stable trot gait. The gait diagram also indicates that the hind legs (RH and LH) had larger duty factors than the front ones (RF and LF) in S2. This indicates that the loads were primarily distributed on the hind legs. Under the vestibular reflex (Fig. 14 (b)), although the joint command offsets were also adjusted when the robot reached the inclined slope, the joint command offsets and  $\bar{\gamma}(n)$  had large variations in five trials (see the shadow area of the joint command and  $\bar{\gamma}(n)$  lines in Fig. 14 (b)). The robot was trapped at the bottom of the slope for the entire test period. This is because the vestibular reflex was stimulated by the body posture feedback rather than  $\bar{\gamma}(n)$ , thereby

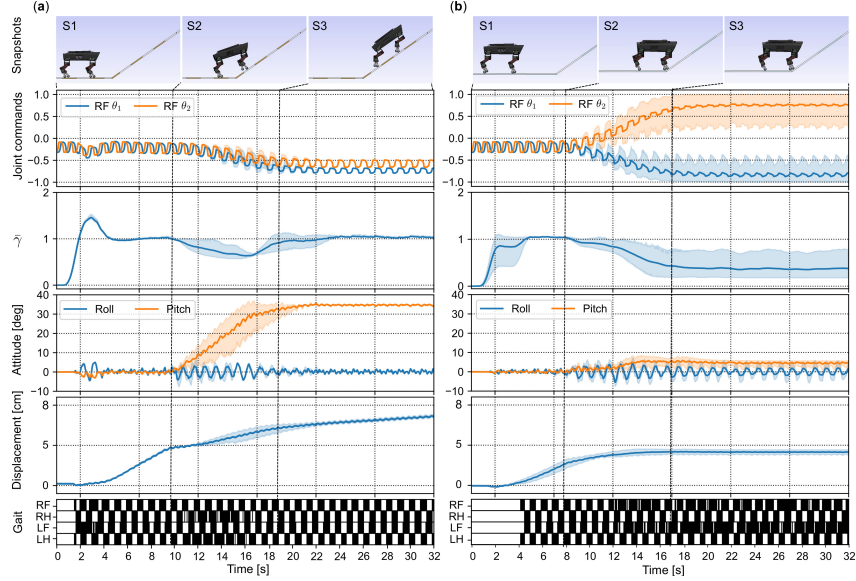


Figure 14: Real-time data for Lilibot trotting from the level ground to the  $35^\circ$  inclined slope.  
(a) Robot controlled by the DFRL. (b) Robot controlled by the vestibular reflex. The black and white regions in the gait diagram indicate the stance and swing phases, respectively. RF, RH, LF, and LH represent the right-front, right-hind, left-front, and left-hind legs, respectively.

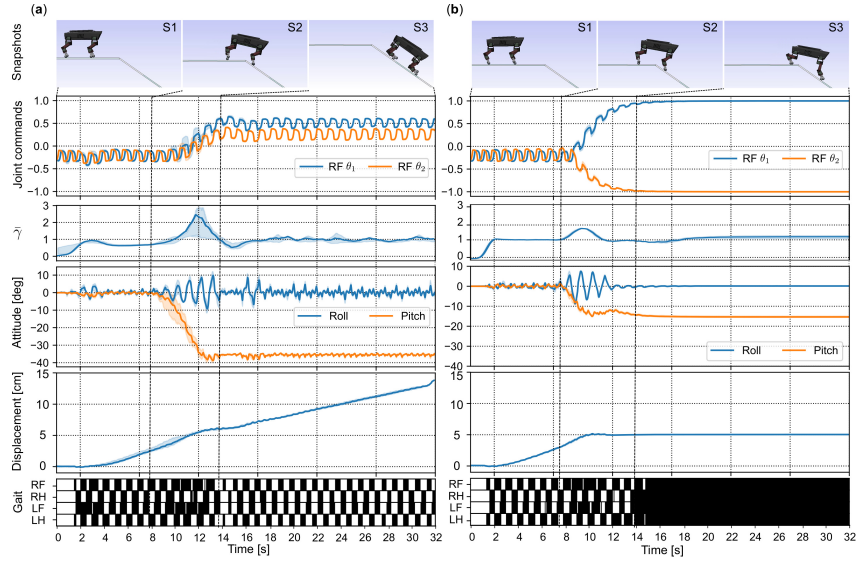


Figure 15: Real-time data for Lilibot trotting from the level ground to the  $35^\circ$  declined slope.  
(a) Robot controlled by the DFRL. (b) Robot controlled by the vestibular reflex. The black and white regions in the gait diagram indicate the stance and swing phases, respectively. RF, RH, LF, and LH represent the right-front, right-hind, left-front, and left-hind legs, respectively.

without suitable adjustment of joint command offsets.

450 The experimental results for the  $-35^\circ$  slope are shown in Fig. 15. Under the DFRL (Fig. 15 (a)), the joint commands and  $\bar{\gamma}(n)$  also quickly converged during the S1 and S3 stages.  $\bar{\gamma}(n)$  was also  $\sim 1.1$ . The pitch angle and displacement curves indicate that the robot successfully trotted forward on the  $-35^\circ$  slope. The gait diagram also exhibits regularity during the S1 and S3 stages.  
455 Conversely, under the vestibular reflex, the robot failed to walk on the  $-35^\circ$  slope (Fig. 15 (b)). This is because the joint commands reached their limits (i.e.,  $\pm 1.0$  rad) under the vestibular reflex, causing the robot to stop.

460 Consequently, the DFRL-based AQMC enables Lilibot to trot stably on steep slopes ( $35^\circ$  and  $-35^\circ$ ), whereas the vestibular-reflex-based AQMC is unable to achieve this.

### 3.3.2. Statistical analysis

Lilibot was controlled by the AQMC (employing either the DFRL or vestibular reflex) and made to trot on every slope terrain five times. The number of times the control was successfully implemented on different slope terrains is  
465 shown in Fig. 16 (a). It shows that the DFRL-controlled Lilibot could trot on all listed slope terrains, whereas the vestibular-reflex-controlled Lilibot could only trot on the  $-10^\circ$ ,  $0^\circ$ ,  $10^\circ$ , and  $20^\circ$  slopes. The statistical locomotion performance of the two reflexes is shown in Figs. 16 (b), (c), and (d).

470 As shown in Fig. 16 (b), the DFRL realized greater stability than the vestibular reflex. Moreover, the steeper the slope, the greater the stability of the DFRL. This is because the step length became shorter on slopes with greater inclination (see joint commands in Fig. 14 (a)). Under the vestibular reflex, robot locomotion exhibited the greatest stability over the flat terrain ( $0^\circ$ ). This is because the initial offsets (i.e., -0.2) of the joint commands were most suitable  
475 for the level ground (see Fig. 13).

As shown in Fig. 16 (c), the DFRL had greater coordination than the vestibular reflex. Furthermore, the DFRL and vestibular reflex both exhibited optimal coordination on the level ground. This is because the initial command

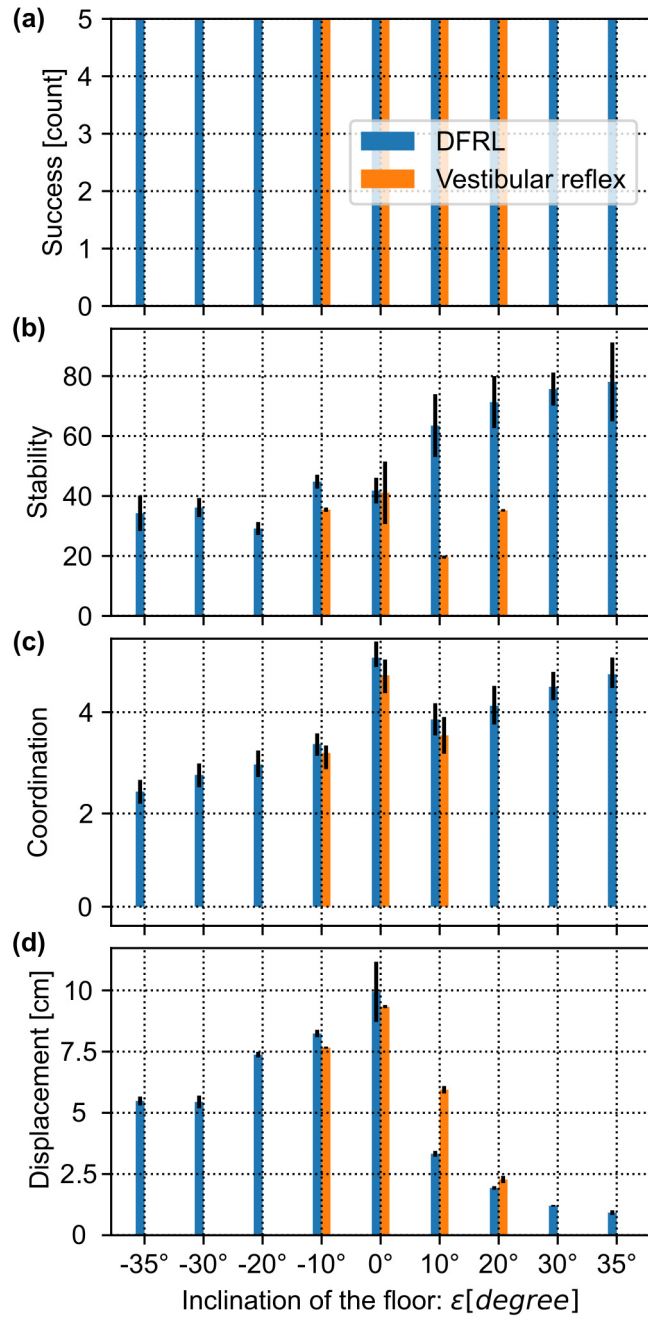


Figure 16: (a) Success count, (b) stability, (c) coordination, and (d) displacement of the robot walking in Experiment II. This demonstrates the comparative results of the DFRL and vestibular reflex.

offsets were most suited to level-ground locomotion, for which the GRF distribution ( $\bar{\gamma}(n)$ ) was already in the desired condition. Moreover, the coordination of the DFRL shows a slight upwards trend over the inclined planes. This is because the robot had a shorter step length on higher inclinations (see joint commands in Fig. 14 (a)), which benefits the coordination to some extent. In addition, the coordination of the vestibular reflex at  $20^\circ$  was zero. This is because the hind legs remained on the ground, even when the robot trotted on the inclined plane. In other words, the hind legs had no swing phase.

Fig. 16 (d) shows that the closer the slope is to the level ground, the longer the displacement under both the DFRL and vestibular reflex. This is because the robot had the greatest coordination and stability and longest step length over the level ground. The displacement on downhill terrains is longer than on uphill ones; this success can be attributed to gravity pushing the robot forward on the downhill whilst pulling the robot on the uphill. Note: the robot using the vestibular reflex on  $10^\circ$  and  $20^\circ$  slopes exhibited a longer displacement than under the DFRL. This is because, on the one hand, the DFRL shortened the step length during uphill locomotion and the stable trot gait on the uphill generated higher foot touch impulse force through its short deceleration process, and on the other hand, the robot under the vestibular reflex generated an irregular trot gait or walking gait, which maintained the robot's constant forward movement.

#### 3.4. Experiment III: trotting on a complex terrain with multiple slopes

In this experiment, the Lilibot controlled by the DFRL-based AQMC was commanded to trot on a complex terrain featuring multiple connected slopes (Fig. 8). This scenario simulates the irregularity of natural ground. From this test, the smoothness of diverse slope transitions can be assessed. Moreover, the locomotion characteristics over different slopes could be consistently compared. A video clip of this experiment can be viewed at <http://www.manoonpong.com/DFFB/video3.mp4>.

The experimental results are shown in Fig. 17. The joint commands of a leg (e.g., the right-front leg) adapted to changes in slope inclinations. The curve

of  $\bar{\gamma}(n)$  indicates the GRF distribution; it shows a significant change during  
510 the terrain transition, while quickly reaching a convergence of  $\sim 1.1$  in non-transition stages. The pitch angle directly reflects the slopes on which the robot is trotting. According to the displacement plot, the locomotion over the declined slopes was faster than that exhibited on inclined ones. The gait diagram clearly shows that the robot exhibited a more regular trot gait when walking on inclined  
515 slopes. This means that the robot achieved a better GRF distribution than that exhibited on the declined slope. To summarize, the DFRL-based AQMC can allow the quadrupedal robot to trot on complex slope terrains.

### 3.5. Generalization test on Laikago

The DFRL-based AQMC was also implemented on Laikago in the simulation.  
520 The control developed for Lilibot (without any modifications) was directly transferred to Laikago. The experimental results show that the proposed control allows Laikago to self-stabilize its body posture (regardless of its initial posture on the level ground) and also trot on different slopes with inclinations of up to  $50^\circ$  (see Fig. 18) and as low as  $-45^\circ$ . A video clip of the experiment can be viewed at <http://www.manoonpong.com/DFFB/video4.mp4>.

## 4. Discussion

In this paper, we propose the AQMC based on the integration of CPGs, sensory feedback, reflex, and online (motor) learning. The control is realized using neural CPG-based control and the DFRL (Fig. 2). The DFRL consists  
530 of a DFFB reflex and DIL. The DFFB reflex is organized as a neural network with synaptic plasticity, and it can adjust the CPG/joint offsets according to the GRF distribution (Fig. 5). The associated DIL is used to online-modulate the plastic synapses ( $w_{1,2}(n)$ , Eq. (12)) of the DFFB reflex network. This improves the DFFB reflex's adaptation speed (Fig. 6). The experimental results show that the DFRL can efficiently generate adaptive CPG/joint offsets and allow quadruped robots to rapidly adapt their postures in response to different initial offsets on the level ground (Experiment I), stably trot on steep  
535

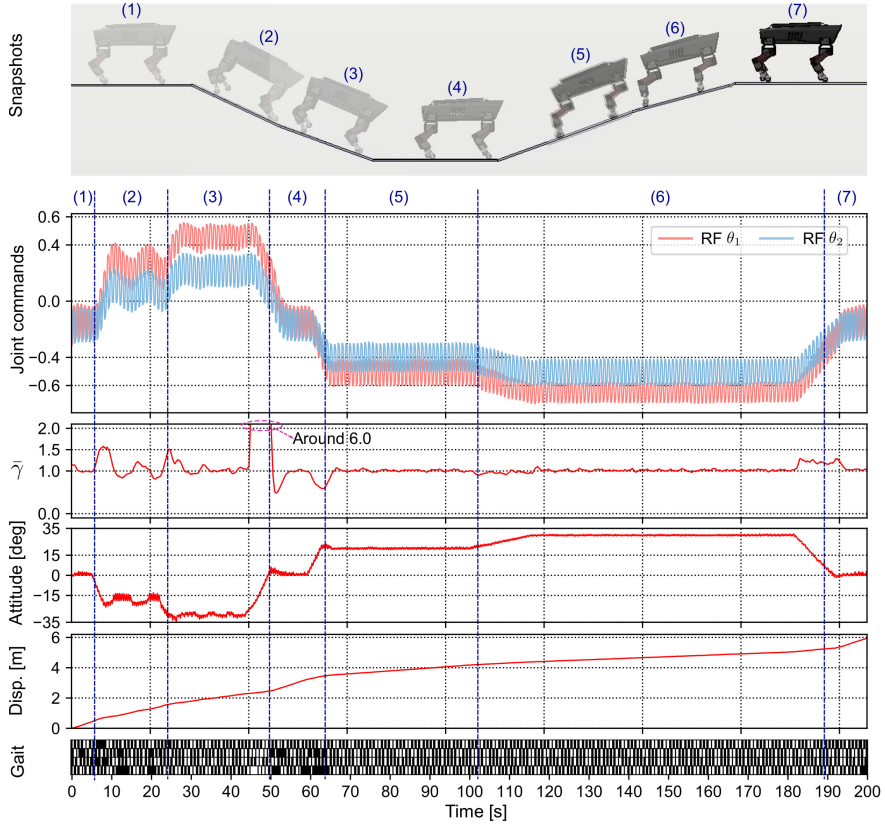


Figure 17: Real-time data of Lilibot trotting on a complex slope terrain. The upper graph refers to the motion scene of the robot and also indicates the complex slope terrain (composed of two flat floors and several declined and inclined slopes). The plots represent the joint commands of a leg (e.g., RF),  $\bar{\gamma}(n)$ , pitch angle of the robot body, displacement of robot locomotion, and gait diagram, respectively. The bars running top to bottom in the gait diagram denote the right-front, right-hind, left-front, and left-hind legs, respectively. The black region represents the stance phase, whilst the white one represents the swing phase.

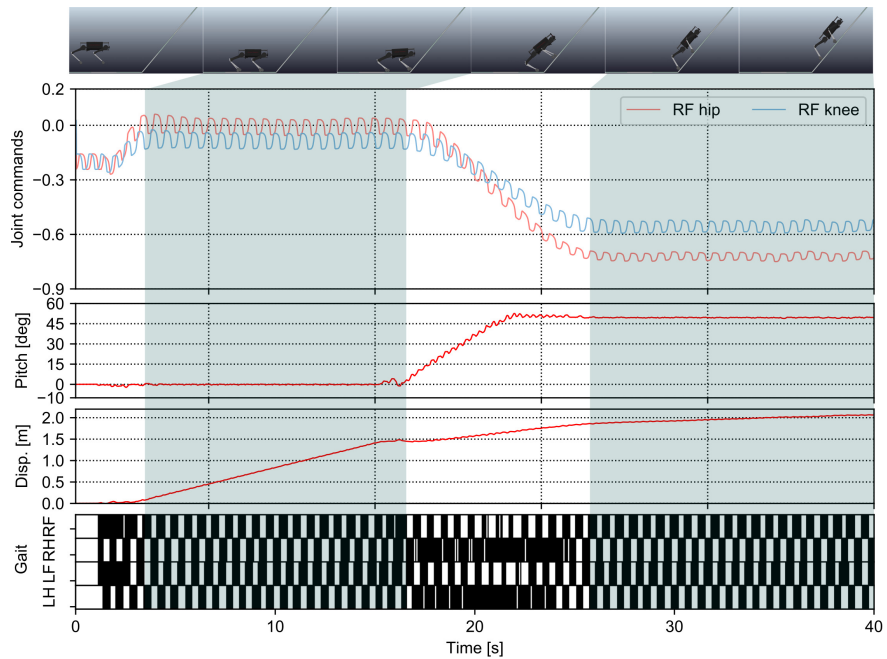


Figure 18: Laikago trotting on a  $50^\circ$  inclined slope. The black regions in the gait diagram represent the stance phase, whilst the white regions represent the swing phase. RF, RH, LF, and LH represent the right-front, right-hind, left-front, and left-hind legs, respectively.

slopes (Experiment II), and properly handle a complex terrain featuring multiple slopes (Experiment III). Moreover, the AQMC developed for Lilibot can be directly implemented on Laikago (Fig. 18). This demonstrates the generalizability of the proposed control to quadruped robots of different sizes and weights, without the need for specific robot models. To summarize, this work concerns two subtopics: (1) realizing CPG/joint offset adaptation using biological mechanisms, to ensure the stable trotting behavior of quadruped robots and (2) applying this CPG/joint offset adaptation on diverse slope terrains. The remaining issues concerning the two subtopics are discussed in the following paragraphs.

A genuine bio-inspired control is model-free, in contrast to engineering-control-based techniques (e.g., whole-body control [6], inverse dynamic model-based control [4], optimization-based control [7], and MPC [8]), and it converges faster than RL approaches [30, 31, 32, 33]. Although several quadruped robots featuring bio-inspired control have achieved such high performances as those reported in well-known works (e.g., BigDog [48], MIT Cheetah [3], and ANYmal [31]), bio-inspired controls have promising potential for generating versatile animal-like movements and promoting biological investigation [1, 10, 49]. Therefore, it is reasonable to expect that a generic, efficient, and adaptive control framework for quadruped robots can be realized through this biologically inspired development route.

To achieve this goal, the DFRL has been developed. Its strategy is inspired by biomechanical findings (i.e., lever mechanics [28]) and aims to maintain a stable body posture over various terrains (Fig. 8). It is constructed using a neural network in which the key synapses ( $w_{1,2}(n)$ ) can be adjusted online via the DIL (Fig. 5). The DIL features two parallel learners with different learning rates (Eq. (11)). This DIL feature provides DFFB plastic synapses with two different time-scale adaptations; moreover, it produces a DFRL with two different level adaptations: internal synapse adaptation (Eq. (12)) and external offset adaptation (Eq. (10)). For instance, when robots traverse over different slopes, their GRF distribution changes; on the one hand, this activates the DFFB re-

flex, which adjusts the robot’s posture; on the other hand, the DIL increases  
570 the network’s synaptic strength, thereby generating high reflex gains. After  
the changes in the GRF distribution have become small, the DIL decreases the  
synaptic strength to generate smaller reflex gains for fine modulation (Fig. 11).  
Synaptic plasticity is relatively useful for overcoming the long delays produced  
575 by the sensory acquisition and preprocessing stages of the DFFB reflex. Otherwise,  
the delay would cause the reflex modulation procedure to become very  
slow with low weights (i.e.,  $w_{1,2}(n)$ ) or unstable with high ones (Fig. 6). The  
functionality of the DIL is analogous to that of serotonin (5-HT) neurons in a bi-  
ological system; these release 5-HT in the spinal cord, to modulate the synaptic  
strengths of interneurons in a locomotive neural network [50, 51, 52, 53, 54].

580 Alongside the flexibility and adaptability realized by the DIL, the DFRL  
is also intrinsically modular and independent of the CPG-model format or the  
size and weight of the robot. The DFRL can be incorporated with SO(2)-based  
CPGs (see Fig. 5) or with dynamical movement primitives-based CPGs [55, 36]  
585 (see Supplementary material), suggesting that the DFRL is generic and applic-  
able to different CPG models. Thus, it is readily integrable with diverse CPG-  
based controls and also facilitates generic adaptive quadruped motor control  
with CPG or joint offset adaptation for different quadruped robots. Furthermore,  
the DFRL can be conveniently integrated with other CPG adaptation  
590 techniques, such as phase [18] or frequency [19] adaptation; this can result in  
CPG-based control with phase, frequency, and offset adaptations, which will  
substantially expand the applicability of bio-inspired CPG-based control. In  
short, this study paves the way for the development of a more advanced bio-  
inspired control mechanism with greater adaptability and generalizability, and  
595 it also sheds some light on neurological locomotion control. Moreover, it demon-  
strates the feasibility of efficiently manipulating sensory information through a  
neural network (with plasticity) to achieve adaptive motor control in robotic  
systems.

However, the DFRL techniques discussed in this paper still feature several  
596 limitations. First, they are limited by the use of the averaged/smoothed GRF

600 distribution  $\bar{\gamma}(n)$  as sensory feedback for the DFFB reflex (see Eq. (9)): Ideally,  
the GRF distribution should be measured whilst the stance/swing phase is being  
switched on, for which the GRF distribution ( $\gamma(n_0)$ ) of a stable trot gait is  
determined as 1.0 (Fig. 4 (b)). Using the averaged GRF distributions results in  
three limitations: (1) it induces an additional empirical parameter (i.e., sample  
605 size  $N$  in Eq. (9)); (2) it produces a larger delay effect in the sensory preprocessing  
module, owing to the moving-average filter; and (3) it decreases robustness  
because the desired  $\bar{\gamma}^d$  (i.e., 1.1) relates to a specific step length and period (see  
Fig. 4 (b)). Therefore, an improved sensory preprocessing module—to obtain  
an instant GRF distribution for a switching moment—should be developed in  
610 future work.

In addition, although the CPG offset adaptation converges rapidly (i.e.,  
within 2 s, see Fig. 6), it cannot handle sudden emergency responses (e.g., to  
prevent the robot from falling due to an unexpected step). Thus, the proposed  
control must be combined with other instant reflexes to tackle such emergencies.  
615 For instance, a flexion reflex can prevent the robot from falling down, sideways  
stepping reflexes can stabilize the rolling motion, and corrective stepping reflexes  
can deal with stepping-down motions [56].

Over the past few decades, quadruped locomotion on slopes has become a  
promising research topic in both animal and robot studies; furthermore, it repre-  
620 sents a necessary function of quadrupeds designed to traverse natural environments  
adaptively [25, 16, 57, 29, 58, 28, 59]. Generally, quadruped locomotion  
on slopes is more complicated than that on the level ground because it involves  
four extra constraints: (1) postural correction, for maintaining balance on slopes  
[28]; (2) flexible joint motion generation, to accommodate transitions between  
625 different terrains (e.g., from flat surfaces to slopes) [60]; (3) a sufficient motor  
power supply, to overcome the effects of appended loads on inclined slopes  
[59]; and (4) an adequate tangential foot force for avoiding slippages caused by  
gravitational compensations on the slope [29]. The former two conditions (i.e.,  
balance and transition) relate to body and joint movement can be managed via  
630 enhanced locomotion control techniques; the latter two conditions (i.e., motor

power and frictional force) depend on robot mechanics and materials. To resolve the two control issues of slope locomotion, a variety of approaches have been proposed and implemented on quadruped robots.

Vestibular reflexes have been proposed in several works; these facilitate adaptive dynamic running over unperceived slopes, where the slopes are regarded as disturbances [22, 23, 24, 25, 16, 26]. More specifically, the vestibular reflex is used to shift the offsets of joint movement commands (originally produced by CPGs), thereby extending or flexing the legs to maintain the robot body parallel to the horizontal (see Fig. S.7 (b)). In addition, Zhao et al. applied a vestibular reflex to adjust the frequency and amplitude of the joint movement commands [27]. This allows the quadruped robot AIBO to trot steadily over slight slopes using a high step frequency and short step length. Despite the successful implementation of vestibular reflexes in these cases, all were limited to gentle slopes (below 20°, see Table 1).

In contrast to vestibular reflexes, the DFFB reflex can translate the ZMP coordination into a proper position along the slope direction. Thus, the robot body's orientation is aligned to the slope when the stability margin is increased (see Fig. S.7 (c)). As a result, the front and hind legs are in a far more natural position to distance themselves from singular configurations or joint limits. Thus, these robots can adapt to steeper slopes. The two distinct strategies (body orientation parallel to the horizontal and parallel to the slope) are referred to in biomechanics as the “telescoping strut” and “lever mechanics”, respectively [28]. Unfortunately, the vestibular reflex cannot realize the lever mechanics strategy because it requires a body orientation parallel to the slope rather than the horizontal. The DFFB reflex is based on the lever mechanics strategy and enables quadruped robots to trot on steep-sloped terrains (e.g., 35° for Lilibot and -45° and 50° for Laikago).

To clarify the relationship between the joint offset and the slope inclination upon which the quadruped robot can trot, we analyze the underlying mechanism using a simplified quadrupedal robot model (see Supplementary material). The analytical model not only proves the functionality of the DFFB reflex strategy

but also predicts the maximum inclination upon which the quadruped robot can trot without considering factors such as friction, joint torque limit, and asymmetric structure. Moreover, the analytical results match the simulation results.

The stability margin for quadruped locomotion can be defined as the minimum distance between the ZMP and support-polygon boundaries [61, 62]. The stability margin of locomotion on the level ground is relatively larger than that on slopes. This is because the ZMP approaches one set of feet when traversing slopes (e.g., the ZMP approaches the hind feet on uphill surfaces and the front feet on downhill ones, see Figs. 4 and S.5). Locomotion stability is affected not only by the joint offsets but also the step length and period (see Fig. 4). The step length determines the motion distance of the ZMP during one step period. In some cases (e.g., when trotting on steep slopes), a small step length is necessary to prevent the ZMP from moving outside the support polygon. In the proposed CPG-based control, the MNs can scale the joint command amplitudes to reduce the step length and height on slopes when the MN offsets are shifted. For instance, when robots trot on a steep slope, the MN offsets are shifted close to the saturation zones of the MN transfer function (i.e., Eq. (5)) owing to the DFFB reflex. As a result, the joint command amplitudes will be decreased, and the robot's step length and height will be reduced. This strategy allows the robot to stabilize its posture during locomotion over slopes (see Figs. 14 and 18). This accords with biomechanical investigations into animal locomotion [63].

We developed the control software based on a standard language (C++) with the robot operating system (ROS) interface. Thus it can be applied to ROS-based quadruped robots. To maximize the contribution and dissemination of our study to the research community, we also provide our control method as open-source software which can be accessed at <https://gitlab.com/neutron-nuaa/dfrl>.

## 5. Conclusion

This paper demonstrates that DFRL-based AQMC can allow quadruped robots to stably trot on diverse slope terrains. This is because the DFRL automatically generates adaptive CPG/joint offsets to ensure a robot posture appropriate to the distribution of GRFs. Moreover, the adaptability and flexibility of the DFRL are significantly improved by the DIL learning mechanism, which online-modulates the reflex gains of the DFFB reflex network of the DFRL. As a result, the DIL provides the DFRL with faster adaptation and greater generalizability across platforms of different sizes and weights (e.g., Lilibot and Laikago).

## Appendix A. Abbreviations and Acronyms

AQMC = Adaptive quadruped motor control.

BBO = Black-box optimization.

CPG(s) = Central pattern generator(s).

DFFB = Distributed-force-feedback-based

DFRL = Distributed-force-feedback-based reflex with online learning

DIL = Dual integral learner

GRF(s) = Ground reaction force(s).

LF = Left-front leg.

LH = Left-hind leg.

MN(s) = Motor neuron(s).

MPC = Model predictive control.

PI2 = Path integrals.

RF = Right-front leg.

RH = Right-hind leg.

RL = Reinforcement learning.

ROS = Robot operation system.

ZMP = Zero moment point.

## Acknowledgment

720 The authors would like to thank Xiaofeng Xiong, Mathias Thor, Weijia Zong,  
Huijuan He, and Chris Bang Sørense for providing fruitful discussions, and Song  
Xu and Yan Li for their comments.

## Role of Funding Sources

725 This work was supported by the NSFC-DFG Collaborative Research Program [Grant No. 51861135306, P.M., project Co-PI] of the National Natural Science Foundation of China, the National Natural Science Foundation of China [Grant No. 51435008 to Z.D], and a CSC Scholarship (Grant No. CSC201906830012) [TS]).

## References

- 730 [1] A. J. Ijspeert, Biorobotics: Using robots to emulate and investigate agile locomotion, *Science* 346 (6206) (2014) 196–203. doi:[10.1126/science.1254486](https://doi.org/10.1126/science.1254486).
- 735 [2] M. Hutter, C. Gehring, D. Jud, A. Lauber, C. D. Bellicoso, V. Tsounis, J. Hwangbo, K. Bodie, P. Fankhauser, M. Bloesch, et al., Anymal-a highly mobile and dynamic quadrupedal robot, in: 2016 IEEE/RSJ International Conference on Intelligent Robots and Systems (IROS), IEEE, 2016, pp. 38–44. doi:[10.1109/IROS.2016.7758092](https://doi.org/10.1109/IROS.2016.7758092).
- 740 [3] G. Bledt, M. J. Powell, B. Katz, J. Di Carlo, P. M. Wensing, S. Kim, Mit cheetah 3: Design and control of a robust, dynamic quadruped robot, in: 2018 IEEE/RSJ International Conference on Intelligent Robots and Systems (IROS), IEEE, 2018, pp. 2245–2252. doi:[10.1109/IROS.2018.8593885](https://doi.org/10.1109/IROS.2018.8593885).
- [4] M. Kalakrishnan, J. Buchli, P. Pastor, M. Mistry, S. Schaal, Learning, planning, and control for quadruped locomotion over challenging terrain,

<sup>745</sup> The International Journal of Robotics Research 30 (2) (2011) 236–258.  
doi:10.1177/0278364910388677.

- [5] C. Semini, V. Barasuol, J. Goldsmith, M. Frigerio, M. Focchi, Y. Gao, D. G. Caldwell, Design of the hydraulically actuated, torque-controlled quadruped robot hyq2max, *IEEE/ASME Transactions on Mechatronics* 22 (2) (2017) 635–646. doi:10.1109/TMECH.2016.2616284.
- <sup>750</sup> [6] M. Hutter, C. Gehring, A. Lauber, F. Gunther, C. D. Bellicoso, V. Tsounis, P. Fankhauser, R. Diethelm, S. Bachmann, M. Blösch, et al., Anymal-toward legged robots for harsh environments, *Advanced Robotics* 31 (17) (2017) 918–931. doi:10.1080/01691864.2017.1378591.
- <sup>755</sup> [7] S. Fahmi, C. Mastalli, M. Focchi, C. Semini, Passive whole-body control for quadruped robots: Experimental validation over challenging terrain, *IEEE Robotics and Automation Letters* 4 (3) (2019) 2553–2560. doi:10.1109/LRA.2019.2908502.
- <sup>760</sup> [8] J. Carlo, P. Wensing, B. Katz, G. Bledt, S. Kim, Dynamic locomotion in the mit cheetah 3 through convex model-predictive control, in: 2018 IEEE/RSJ International Conference on Intelligent Robots and Systems (IROS), 2018, pp. 1–9. doi:10.1109/IROS.2018.8594448.
- <sup>765</sup> [9] P. Manoonpong, U. Parlitz, F. Wrgtter, Neural control and adaptive neural forward models for insect-like, energy-efficient, and adaptable locomotion of walking machines, *Frontiers in Neural Circuits* 7 (2013) 12. doi:10.3389/fncir.2013.00012.
- [10] A. J. Ijspeert, Central pattern generators for locomotion control in animals and robots: a review, *Neural Networks* 21 (4) (2008) 642–653. doi:10.1016/j.neunet.2008.03.014.
- <sup>770</sup> [11] J. H. Barron-Zambrano, C. Torres-Huitzil, Fpga implementation of a configurable neuromorphic cpg-based locomotion controller, *Neural Networks* 45 (2013) 50 – 61. doi:10.1016/j.neunet.2013.04.005.

- [12] M. R. Dimitrijevic, Y. Gerasimenko, M. M. Pinter, Evidence for a spinal central pattern generator in humans, *Annals of the New York Academy of Sciences* 860 (1) (1998) 360–376. doi:[10.1111/j.1749-6632.1998.tb09062.x](https://doi.org/10.1111/j.1749-6632.1998.tb09062.x).
- [13] E. Marder, D. Bucher, Central pattern generators and the control of rhythmic movements, *Current Biology* 11 (23) (2001) R986–R996. doi:[10.1016/S0960-9822\(01\)00581-4](https://doi.org/10.1016/S0960-9822(01)00581-4).
- [14] M. MacKay-Lyons, Central pattern generation of locomotion: a review of the evidence, *Physical Therapy* 82 (1) (2002) 69–83. doi:[10.1093/ptj/82.1.69](https://doi.org/10.1093/ptj/82.1.69).
- [15] A. J. Ijspeert, A. Crespi, D. Ryczko, J.-M. Cabelguen, From swimming to walking with a salamander robot driven by a spinal cord model, *Science* 315 (5817) (2007) 1416–1420. doi:[10.1126/science.1138353](https://doi.org/10.1126/science.1138353).
- [16] Y. Fukuoka, H. Kimura, A. H. Cohen, Adaptive dynamic walking of a quadruped robot on irregular terrain based on biological concepts, *The International Journal of Robotics Research* 22 (3-4) (2003) 187–202. doi:[10.1177/0278364907078089](https://doi.org/10.1177/0278364907078089).
- [17] D. Owaki, T. Kano, K. Nagasawa, A. Tero, A. Ishiguro, Simple robot suggests physical interlimb communication is essential for quadruped walking, *Journal of The Royal Society Interface* 10 (78) (2013) 20120669. doi:[10.1098/rsif.2012.0669](https://doi.org/10.1098/rsif.2012.0669).
- [18] T. Sun, D. Shao, Z. Dai, P. Manoonpong, Adaptive neural control for self-organized locomotion and obstacle negotiation of quadruped robots, in: 2018 27th IEEE International Symposium on Robot and Human Interactive Communication (RO-MAN), IEEE, 2018, pp. 1081–1086. doi:[10.1109/ROMAN.2018.8525645](https://doi.org/10.1109/ROMAN.2018.8525645).
- [19] M. Thor, P. Manoonpong, Error-based learning mechanism for fast online adaptation in robot motor control, *IEEE Transactions on Neural Networks*

and Learning Systems 31 (6) (2020) 2042–2051. doi:10.1109/TNNLS.2019.2927737.

- [20] K. Matsuoka, Mechanisms of frequency and pattern control in the neural rhythm generators, *Biological Cybernetics* 56 (5-6) (1987) 345–353. doi:10.1007/BF00319514.
- [21] D. T. Tran, I. M. Koo, Y. H. Lee, H. Moon, S. Park, J. C. Koo, H. R. Choi, Central pattern generator based reflexive control of quadruped walking robots using a recurrent neural network, *Robotics and Autonomous Systems* 62 (10) (2014) 1497–1516. doi:10.1016/j.robot.2014.05.011.
- [22] C. Liu, L. Xia, C. Zhang, Q. Chen, Multi-layered cpg for adaptive walking of quadruped robots, *Journal of Bionic Engineering* 15 (2) (2018) 341–355. doi:10.1007/s42235-018-0026-8.
- [23] X. Zhang, H. Zheng, Walking up and down hill with a biologically-inspired postural reflex in a quadrupedal robot, *Autonomous Robots* 25 (1-2) (2008) 15–24. doi:10.1007/s10514-007-9072-5.
- [24] J. Sousa, V. Matos, C. P. dos Santos, A bio-inspired postural control for a quadruped robot: an attractor-based dynamics, in: 2010 IEEE/RSJ International Conference on Intelligent Robots and Systems, IEEE, 2010, pp. 5329–5334. doi:10.1109/IROS.2010.5648945.
- [25] M. Ajallooeian, S. Pouya, A. Sproewitz, A. J. Ijspeert, Central pattern generators augmented with virtual model control for quadruped rough terrain locomotion, in: 2013 IEEE international conference on robotics and automation, IEEE, 2013, pp. 3321–3328. doi:10.1109/ICRA.2013.6631040.
- [26] T. Sun, X. Xiong, Z. Dai, P. Manoonpong, Small-sized reconfigurable quadruped robot with multiple sensory feedback for studying adaptive and versatile behaviors, *Frontiers in Neurorobotics* 14 (2020) 14. doi:10.3389/fnbot.2020.00014.

- [27] X. Zhao, J. Zhang, C. Qi, Cpg and reflexes combined adaptive walking control for aibo, in: 2012 11th International Conference on Machine Learning and Applications, Vol. 1, IEEE, 2012, pp. 448–453. doi: [10.1109/ICMLA.2012.81](https://doi.org/10.1109/ICMLA.2012.81).
- [28] D. V. Lee, Effects of grade and mass distribution on the mechanics of trotting in dogs, *Journal of Experimental Biology* 214 (3) (2011) 402–411.
- [29] C. Gehring, C. D. Bellicoso, S. Coros, M. Bloesch, P. Fankhauser, M. Hutter, R. Siegwart, Dynamic trotting on slopes for quadrupedal robots, in: 2015 IEEE/RSJ International Conference on Intelligent Robots and Systems (IROS), IEEE, 2015, pp. 5129–5135. doi: [10.1109/IROS.2015.7354099](https://doi.org/10.1109/IROS.2015.7354099).
- [30] N. Heess, D. TB, S. Sriram, J. Lemmon, J. Merel, G. Wayne, Y. Tassa, T. Erez, Z. Wang, S. M. A. Eslami, M. Riedmiller, D. Silver, Emergence of locomotion behaviours in rich environments (2017). [arXiv:1707.02286](https://arxiv.org/abs/1707.02286).
- [31] J. Hwangbo, J. Lee, A. Dosovitskiy, D. Bellicoso, V. Tsounis, V. Koltun, M. Hutter, Learning agile and dynamic motor skills for legged robots, *Science Robotics* 4 (26). doi: [10.1126/scirobotics.aau5872](https://doi.org/10.1126/scirobotics.aau5872).
- [32] W. Jones, T. Blum, K. Yoshida, Adaptive slope locomotion with deep reinforcement learning, in: 2020 IEEE/SICE International Symposium on System Integration (SII), IEEE, 2020, pp. 546–550. doi: [10.1109/SII46433.2020.9025928](https://doi.org/10.1109/SII46433.2020.9025928).
- [33] M. Thor, T. Kulvicius, P. Manoonpong, Generic neural locomotion control framework for legged robots, *IEEE Transactions on Neural Networks and Learning Systems* (2020) 1–13 doi: [10.1109/TNNLS.2020.3016523](https://doi.org/10.1109/TNNLS.2020.3016523).
- [34] Y. Nakamura, T. Mori, M. aki Sato, S. Ishii, Reinforcement learning for a biped robot based on a cpg-actor-critic method, *Neural Networks* 20 (6) (2007) 723 – 735. doi: [10.1016/j.neunet.2007.01.002](https://doi.org/10.1016/j.neunet.2007.01.002).

- 855 [35] F. Pasemann, M. Hild, K. Zahedi, So(2)-networks as neural oscillators, in: Computational Methods in Neural Modeling, Springer Berlin Heidelberg, Berlin, Heidelberg, 2003, pp. 144–151. doi:[10.1007/3-540-44868-3\\_19](https://doi.org/10.1007/3-540-44868-3_19).
- 860 [36] A. J. Ijspeert, J. Nakanishi, H. Hoffmann, P. Pastor, S. Schaal, Dynamical movement primitives: learning attractor models for motor behaviors, *Neural Computation* 25 (2) (2013) 328–373. doi:[10.1162/NECO\\_a\\_00393](https://doi.org/10.1162/NECO_a_00393).
- 865 [37] S. Aoi, T. Yamashita, K. Tsuchiya, Hysteresis in the gait transition of a quadruped investigated using simple body mechanical and oscillator network models, *Physical Review E* 83 (6) (2011) 061909. doi:[10.1103/PhysRevE.83.061909](https://doi.org/10.1103/PhysRevE.83.061909).
- [38] T. Ichinomiya, Frequency synchronization in a random oscillator network, *Physical Review E* 70 (2004) 026116. doi:[10.1103/PhysRevE.70.026116](https://doi.org/10.1103/PhysRevE.70.026116).
- 870 [39] G. Schnier, W. Jiang, J. Kelso, A synergetic theory of quadrupedal gaits and gait transitions, *Journal of Theoretical Biology* 142 (3) (1990) 359 – 391. doi:[10.1016/S0022-5193\(05\)80558-2](https://doi.org/10.1016/S0022-5193(05)80558-2).
- [40] T. Aoki, T. Aoyagi, Co-evolution of phases and connection strengths in a network of phase oscillators, *Physical Review Letter* 102 (2009) 034101. doi:[10.1103/PhysRevLett.102.034101](https://doi.org/10.1103/PhysRevLett.102.034101).
- 875 [41] I. Z. Kiss, Y. Zhai, J. L. Hudson, Emerging coherence in a population of chemical oscillators, *Science* 296 (5573) (2002) 1676–1678. doi:[10.1126/science.1070757](https://doi.org/10.1126/science.1070757).
- [42] L. Righetti, J. Buchli, M. Mistry, M. Kalakrishnan, S. Schaal, Optimal distribution of contact forces with inverse-dynamics control, *The International Journal of Robotics Research* 32 (3) (2013) 280–298. doi:[10.1177/0278364912469821](https://doi.org/10.1177/0278364912469821).
- 880 [43] Z. Li, S. S. Ge, S. Liu, Contact-force distribution optimization and control for quadruped robots using both gradient and adaptive neural networks,

- IEEE Transactions on Neural Networks and Learning Systems 25 (8) (2013) 1460–1473. doi:10.1109/TNNLS.2013.2293500.
- [44] J. H. Lee, J. H. Park, Optimization of postural transition scheme for quadruped robots trotting on various surfaces, IEEE Access 7 (2019) 168126–168140. doi:10.1109/ACCESS.2019.2954489.
- [45] M. Vukobratović, B. Borovac, Zero-moment point thirty five years of its life, International Journal of Humanoid Robotics 1 (01) (2004) 157–173. doi:10.1142/S0219843604000083.
- [46] J. R. Hughes, Post-tetanic potentiation, Physiological Reviews 38 (1) (1958) 91–113. doi:10.1152/physrev.1958.38.1.91.
- [47] C. Yu, L. Zhou, H. Qian, Y. Xu, Posture correction of quadruped robot for adaptive slope walking, in: 2018 IEEE International Conference on Robotics and Biomimetics (ROBIO), IEEE, 2018, pp. 1220–1225. doi:10.1109/ROBIO.2018.8665093.
- [48] M. Raibert, K. Blankespoor, G. Nelson, R. Playter, Bigdog, the rough-terrain quadruped robot, IFAC Proceedings Volumes 41 (2) (2008) 10822–10825. doi:10.3182/20080706-5-KR-1001.01833.
- [49] G. Urbain, V. Barasuol, C. Semini, J. Dambre, F. wyffels, Stance control inspired by cerebellum stabilizes reflex-based locomotion on hyq robot (2020). arXiv:2003.09327.
- [50] G. E. Stutzmann, B. S. McEwen, J. E. LeDoux, Serotonin modulation of sensory inputs to the lateral amygdala: dependency on corticosterone, Journal of Neuroscience 18 (22) (1998) 9529–9538. doi:10.1523/JNEUROSCI.18-22-09529.1998.
- [51] T. Deemyad, M. G. Metzen, Y. Pan, M. J. Chacron, Serotonin selectively enhances perception and sensory neural responses to stimuli generated by same-sex conspecifics, Proceedings of the National Academy of Sciences 110 (48) (2013) 19609–19614. doi:10.1073/pnas.1314008110.

- 910 [52] E. Lottem, M. L. Lörincz, Z. F. Mainen, Optogenetic activation of dorsal raphe serotonin neurons rapidly inhibits spontaneous but not odor-evoked activity in olfactory cortex, *Journal of Neuroscience* 36 (1) (2016) 7–18. [doi:10.1523/JNEUROSCI.3008-15.2016](https://doi.org/10.1523/JNEUROSCI.3008-15.2016).
- 915 [53] M. C. Avery, J. L. Krichmar, Neuromodulatory systems and their interactions: A review of models, theories, and experiments, *Frontiers in Neural Circuits* 11 (2017) 108. [doi:10.3389/fncir.2017.00108](https://doi.org/10.3389/fncir.2017.00108).
- [54] U. Sawiska, L. M. Jordan, Serotonergic influences on locomotor circuits, *Current Opinion in Physiology* 8 (2019) 63 – 69. [doi:10.1016/j.cophys.2018.12.012](https://doi.org/10.1016/j.cophys.2018.12.012).
- 920 [55] J. Nakanishi, J. Morimoto, G. Endo, G. Cheng, S. Schaal, M. Kawato, A framework for learning biped locomotion with dynamical movement primitives, in: 4th IEEE/RAS International Conference on Humanoid Robots, 2004., Vol. 2, IEEE, 2004, pp. 925–940. [doi:10.1109/ICHR.2004.1442695](https://doi.org/10.1109/ICHR.2004.1442695).
- 925 [56] H. Kimura, Y. Fukuoka, A. H. Cohen, Adaptive dynamic walking of a quadruped robot on natural ground based on biological concepts, *The International Journal of Robotics Research* 26 (5) (2007) 475–490. [doi:10.1177/0278364907078089](https://doi.org/10.1177/0278364907078089).
- 930 [57] R. Hodoshima, T. Doi, Y. Fukuda, S. Hirose, T. Okamoto, J. Mori, Development of titan xi: a quadruped walking robot to work on slopes, in: 2004 IEEE/RSJ International Conference on Intelligent Robots and Systems (IROS), Vol. 1, IEEE, 2004, pp. 792–797. [doi:10.1109/IROS.2004.1389449](https://doi.org/10.1109/IROS.2004.1389449).
- 935 [58] J. He, J. Shao, G. Sun, X. Shao, Survey of quadruped robots coping strategies in complex situations, *Electronics* 8 (12) (2019) 1414. [doi:10.3390/electronics8121414](https://doi.org/10.3390/electronics8121414).
- [59] D. J. Dutto, D. F. Hoyt, E. A. Cogger, S. J. Wickler, Ground reaction forces in horses trotting up an incline and on the level over a range of

- speeds, *Journal of Experimental Biology* 207 (20) (2004) 3507–3514. doi:  
10.1242/jeb.01171.
- [60] Y. N. G. Hong, J. Lee, C. S. Shin, Transition versus continuous slope walking: adaptation to change center of mass velocity in young men, *Applied Bionics and Biomechanics* 2018. doi:10.1155/2018/2028638.
- [61] Y. Jia, X. Luo, B. Han, G. Liang, J. Zhao, Y. Zhao, Stability criterion for dynamic gaits of quadruped robot, *Applied Sciences* 8 (12) (2018) 2381. doi:10.3390/app8122381.
- [62] H. Hirukawa, S. Hattori, K. Harada, S. Kajita, K. Kaneko, F. Kanehiro, K. Fujiwara, M. Morisawa, A universal stability criterion of the foot contact of legged robots-adios zmp, in: *Proceedings 2006 IEEE International Conference on Robotics and Automation, 2006. ICRA 2006.*, IEEE, 2006, pp. 1976–1983. doi:10.1109/ROBOT.2006.1641995.
- [63] Z.-Y. Wang, A.-H. Ji, T. Endlein, W. Li, D. Samuel, Z.-D. Dai, Locomotor kinematics of the gecko (tokay gecko) upon challenge with various inclines, *Chinese Science Bulletin* 59 (33) (2014) 4568–4577. doi:10.1007/s11434-014-0557-2.